

Resolution analysis for imaging with noise

Josselin Garnier¹ and George Papanicolaou²

¹ Laboratoire de Probabilités et Modèles Aléatoires & Laboratoire Jacques-Louis Lions, Université Paris VII, 2 Place Jussieu, 75251 Paris Cedex 5, France

²Mathematics Department, Stanford University, Stanford, CA 94305

E-mail: papanico@math.stanford.edu, garnier@math.jussieu.fr

Abstract. We analyze the resolution of imaging functionals that migrate the cross correlation matrices of passive sensor arrays. These matrices are obtained by cross correlating signals emitted by ambient noise sources and recorded by the passive sensor array. They contain information about reflectors in the surrounding medium. Therefore, travel time or Kirchhoff migration of the cross correlations can, under favorable circumstances, produce images of such reflectors. However migration should be carried out appropriately depending on the type of illumination provided by the ambient noise sources. We present here a detailed resolution analysis of these functionals in a homogeneous medium. Resolution depends on the sensor array diameter, the distance from the array to the reflector and the central frequency, as is the case in active array imaging. When imaging with passive sensor arrays and ambient noise, resolution also depends on the space and time coherence of the noise sources because it determines an effective noise bandwidth.

PACS numbers: 43.60.Cg, 43.60.Pt, 43.60.Gk, 42.30.Wb

Submitted to: *Inverse Problems*

1. Introduction

The detection and location of wave reflectors from coherent wave measurements is a central issue in imaging. To image reflectors with an active sensor array located at $\{\mathbf{x}_j\}_{j=1,\dots,N}$ one first records the impulse response matrix $(P(t, \mathbf{x}_j, \mathbf{x}_l))_{j,l=1,\dots,N,t \in \mathbb{R}}$ of the array and then one gets an image using travel time or Kirchhoff migration. The (j, l) -th element $(P(t, \mathbf{x}_j, \mathbf{x}_l))_{t \in \mathbb{R}}$ of the impulse response matrix is the signal recorded by the sensor \mathbf{x}_j when the sensor \mathbf{x}_l emits an impulse. To form an image, each element of the impulse response matrix is evaluated at the sum of the travel times $\mathcal{T}(\mathbf{x}_l, \mathbf{z}^S) + \mathcal{T}(\mathbf{z}^S, \mathbf{x}_j)$ between the emitting sensor \mathbf{x}_l and a search point \mathbf{z}^S in the image domain, and between the search point \mathbf{z}^S and the receiving sensor \mathbf{x}_j . The Kirchhoff migration imaging functional is then the sum of the migrated matrix elements over all emitters and receivers. This works because the (j, l) -th element of the impulse response matrix has peaks at the sum of the travel times $\mathcal{T}(\mathbf{x}_l, \mathbf{z}_r) + \mathcal{T}(\mathbf{z}_r, \mathbf{x}_j)$ between the emitting sensor \mathbf{x}_l and a localized reflector at \mathbf{z}_r , and between the reflector and the receiving sensor \mathbf{x}_j .

It was pointed out in [7, 1, 12] that such travel time information is also contained in the cross correlation of signals recorded by the sensor array when the reflectors are illuminated only by ambient noise sources. Therefore reflectors can be imaged by suitably migrating cross correlations of noise signals recorded by passive sensor arrays. We mean by this that (a) the imaging functional will depend on the positions of the reflectors relative to the array and to the region occupied by the noise sources, and (b) reference cross correlations must be available in the absence of the reflectors so that differences of cross correlations can be formed and migrated. The relative position of the sensor array, the reflectors, and the noise source region plays a role because the peaks of the cross correlation may not be at the sum of the travel times described above but at their difference, corresponding to what was called daylight and backlight illuminations in [12], respectively. Using the difference of the cross correlations is important because the peaks that are relevant in imaging localized reflectors are much weaker than the peaks of cross correlations at inter-sensor travel times, which must therefore be removed.

The purpose of this paper is to carry out a detailed resolution analysis of correlation based imaging functionals, in a homogeneous medium. The analysis is based on a systematic use of the stationary phase method where the large parameter is the ratio of the typical travel time of interest to the coherence time of the ambient noise sources. We show that resolution depends on the sensor array diameter, the distance from the array to the reflector and the central frequency, as is the case in active array imaging. However, when imaging with passive sensor arrays and ambient noise, as in this paper, resolution also depends on the space and time coherence of the noise sources because it determines an effective noise bandwidth.

The resolution formulas obtained in this paper are useful for various applications of passive interferometric imaging. Cross correlations of signals emitted by ambient noise sources and recorded by a passive sensor array have recently been used to estimate the

Green's function of the wave equation in homogeneous and inhomogeneous media. In particular, the cross correlation of the recorded signals by a pair of passive sensors has been shown to provide a reliable estimate of the Green's function, and hence the travel time, between them. In geophysics this can be used to carry out a tomographic surface wave velocity estimation [15], as was done in the Southern California region [17], in Tibet [23], and in the Alps [21]. The idea of using the cross correlation of noise signals to get information about travel times was first used in helioseismology and seismology [10, 16, 19]. It has been applied to seismic data ranging from regional to local scales [15, 20, 14], for volcano monitoring [18, 6], and for reservoir monitoring [8]. So far most applications of cross correlation techniques with passive sensor data are in geophysics. However we expect that they should be useful in other contexts, in microwave regimes in particular. For instance, wireless cell phones in an urban or indoor environment could be considered as statistically stationary, spatially distributed noise sources. The resolution analysis in this case is especially important as the bandwidth (20 MHz) is relatively small compared to the central frequency of (2.4 GHz).

The paper is organized as follows. In Section 2 we review the background from [12] that we need here. In Section 3 we present the imaging functionals and their resolution analysis, which is the main result of the paper. We conclude with a brief summary and conclusions. The analytical details, based on the stationary phase method, are given in the Appendices.

2. Imaging by cross correlation of noisy signals

2.1. The wave equation with noise sources

We consider the solution u of the wave equation in a three-dimensional inhomogeneous medium with propagation speed $c(\mathbf{x})$:

$$\frac{1}{c^2(\mathbf{x})} \frac{\partial^2 u}{\partial t^2} - \Delta_{\mathbf{x}} u = n(t, \mathbf{x}), \quad (1)$$

along with a radiation condition at infinity and given initial conditions. The term $n(t, \mathbf{x})$ models a random distribution of noise sources. It is a zero-mean stationary (in time) random process with autocorrelation function

$$\langle n(t_1, \mathbf{y}_1) n(t_2, \mathbf{y}_2) \rangle = F(t_2 - t_1) K\left(\frac{\mathbf{y}_1 + \mathbf{y}_2}{2}\right) H(\mathbf{y}_2 - \mathbf{y}_1). \quad (2)$$

Here $\langle \cdot \rangle$ stands for statistical average with respect to the law of the noise sources. For simplicity we assume that the random field $n(t, \mathbf{x})$ is Gaussian and that the autocorrelation function on the right in (2) factors as indicated.

The time distribution of the noise sources is characterized by the correlation function $F(t_2 - t_1)$, which is a function of $t_2 - t_1$ only by time stationarity. It is even and takes its maximum at 0. It is normalized so that $F(0) = 1$. Its Fourier transform $\hat{F}(\omega)$ is a nonnegative real-valued even function, proportional to the power spectral density

of the sources:

$$\hat{F}(\omega) = \int F(t)e^{i\omega t} dt. \quad (3)$$

The spatial distribution of the noise sources is characterized by the autocovariance function $K((\mathbf{y}_1 + \mathbf{y}_2)/2)H(\mathbf{y}_2 - \mathbf{y}_1)$. The function K determines the spatial support of the sources and it is assumed to be smooth and compactly supported. The function H is the local covariance function. It is normalized so that $H(\mathbf{0}) = 1$ and its Fourier transform

$$\hat{H}(\mathbf{k}) = \int H(\mathbf{y})e^{-i\mathbf{k}\cdot\mathbf{y}} d\mathbf{y} \quad (4)$$

is assumed to be nonnegative, even, and isotropic (i.e. it depends only on the modulus $|\mathbf{k}|$). A typical situation is when K and H have Gaussian profiles with radii R_0 (the radius of the source region) and ρ_c (the correlation radius of the sources), respectively. Both the time correlation function F and the spatial covariance function H play a role in the resolution analysis.

2.2. Statistical stability of the cross correlation function

The stationary in time solution of the wave equation has the integral representation

$$u(t, \mathbf{x}) = \iint n(t-s, \mathbf{y})G(s, \mathbf{x}, \mathbf{y}) ds d\mathbf{y}, \quad (5)$$

where $G(t, \mathbf{x}, \mathbf{y})$ is the time-dependent causal Green's function. It is the fundamental solution of the wave equation

$$\frac{1}{c^2(\mathbf{x})} \frac{\partial^2 G}{\partial t^2} - \Delta_{\mathbf{x}} G = \delta(t)\delta(\mathbf{x} - \mathbf{y}), \quad (6)$$

starting from $G(0, \mathbf{x}, \mathbf{y}) = \partial_t G(0, \mathbf{x}, \mathbf{y}) = 0$, and continued on the negative time axis by $G(t, \mathbf{x}, \mathbf{y}) = 0 \forall t \leq 0$.

The empirical cross correlation over $(0, T)$ of the signals recorded at \mathbf{x}_1 and \mathbf{x}_2 is defined by

$$C_T(\tau, \mathbf{x}_1, \mathbf{x}_2) = \frac{1}{T} \int_0^T u(t, \mathbf{x}_1)u(t+\tau, \mathbf{x}_2) dt. \quad (7)$$

It is a statistically stable quantity, in the sense that for a large integration time T the empirical cross correlation C_T is independent of the realization of the noise sources. This is stated in the following proposition, which is an extension of Proposition 4.1 in [12] where the limiting delta-correlated case $H(\mathbf{z}) = \delta(\mathbf{z})$ is considered.

Proposition 2.1 *1. The expectation of the empirical cross correlation C_T (with respect to the statistical law of the sources) is independent of T :*

$$\langle C_T(\tau, \mathbf{x}_1, \mathbf{x}_2) \rangle = C^{(1)}(\tau, \mathbf{x}_1, \mathbf{x}_2). \quad (8)$$

The theoretical (or statistical) cross correlation $C^{(1)}$ is given by

$$C^{(1)}(\tau, \mathbf{x}_1, \mathbf{x}_2) = \frac{1}{2\pi} \iiint d\mathbf{y} d\mathbf{z} d\omega \hat{F}(\omega) K(\mathbf{y}) H(\mathbf{z}) \\ \times \hat{G}\left(\omega, \mathbf{x}_1, \mathbf{y} + \frac{\mathbf{z}}{2}\right) \hat{G}\left(\omega, \mathbf{x}_2, \mathbf{y} - \frac{\mathbf{z}}{2}\right) \exp(-i\omega\tau), \quad (9)$$

where $\hat{G}(\omega, \mathbf{x}, \mathbf{y})$ is the time-harmonic Green's function, that is, the Fourier transform of $G(t, \mathbf{x}, \mathbf{y})$, and the $\bar{\cdot}$ stands for complex conjugation.

2. The empirical cross correlation C_T is a self-averaging quantity:

$$C_T(\tau, \mathbf{x}_1, \mathbf{x}_2) \xrightarrow{T \rightarrow \infty} C^{(1)}(\tau, \mathbf{x}_1, \mathbf{x}_2), \quad (10)$$

in probability with respect to the statistical law of the sources.

2.3. Passive sensor imaging

We review briefly passive sensor imaging using cross correlations as presented in more detail in [12].

Consider an array of sensors located at $(\mathbf{x}_j)_{j=1, \dots, N}$ and small reflectors (i.e. local changes in the the speed of propagation as described in Appendix A) located at $(\mathbf{z}_{r,j})_{j=1, \dots, N_r}$. In imaging we want to estimate the locations of the reflectors from the signals recorded by the sensors. The data set used in sensor imaging is the impulse response matrix $(P(t, \mathbf{x}_j, \mathbf{x}_l))_{j,l=1, \dots, N, t \in \mathbb{R}}$. The (j, l) -entry of this matrix is the signal $(P(t, \mathbf{x}_j, \mathbf{x}_l))_{t \in \mathbb{R}}$ recorded by the j th sensor when the l th sensor emits a Dirac impulse. When the impulse response matrix $(P(t, \mathbf{x}_j, \mathbf{x}_l))_{j,l=1, \dots, N, t \in \mathbb{R}}$ of the sensor array is known, even partially, then the usual travel time migration techniques [2, 3] that backpropagate the impulse responses numerically in a fictitious medium give estimates of the locations of the reflectors.

In *active* sensor imaging, the sensors of the array can be used as emitters as well as receivers, and we obtain directly the signal $(P(t, \mathbf{x}_j, \mathbf{x}_l))_{t \in \mathbb{R}}$ recorded by the j th sensor when the l th sensor emits a short impulse. However, in *passive* sensor imaging, the sensors of the array do not have emission capacity and they can only be used as receivers. In this paper we assume that the only available data are the signals $(u(t, \mathbf{x}_j))_{t \in \mathbb{R}}$ emitted by ambient noise sources and recorded by the j th sensor for $j = 1, \dots, N$. It was shown in [12], and will be shown in more detail in the next Section 3, that the impulse response matrix of a passive sensor array can be estimated from the matrix of cross correlations of the recorded signals $(C(\tau, \mathbf{x}_j, \mathbf{x}_l))_{j,l=1, \dots, N, \tau \in \mathbb{R}}$ (with C defined as in (7)). This is because the cross correlation between two sensors has peaks at time lags corresponding to travel times between the sensors and the reflectors. It is therefore possible to image the reflectors by migrating the cross correlations.

In order to image the reflectors, we assume that we know the travel times $\mathcal{T}(\mathbf{x}, \mathbf{y})$ between the sensors \mathbf{x} and points \mathbf{y} in the search region around the reflectors to be imaged. If in particular the medium is homogeneous, as we assume here, then $\mathcal{T}(\mathbf{x}, \mathbf{y}) = |\mathbf{x} - \mathbf{y}|/c_0$. We also assume that data sets $\{C(\tau, \mathbf{x}_j, \mathbf{x}_l)\}_{j,l=1, \dots, N}$ and $\{C_0(\tau, \mathbf{x}_j, \mathbf{x}_l)\}_{j,l=1, \dots, N}$, with and without the reflectors, respectively, are available so

that we can compute the differential cross correlations $\{C - C_0\}$ and migrate them. It may not be possible to image with only primary data set $\{C\}$. This is because peaks in the cross correlations associated with the reflectors are weak compared to the contribution of the direct waves [12]. When the contributions of the waves interacting with the reflectors and the ones coming directly from the sources can be separated in the cross correlation C , then it is possible to use the same imaging functionals. This is the case in daylight configurations, in which the contributions of the direct waves in $C(\tau, \mathbf{x}_j, \mathbf{x}_l)$ is concentrated within the interval $\tau \in [-\mathcal{T}(\mathbf{x}_j, \mathbf{x}_l), \mathcal{T}(\mathbf{x}_j, \mathbf{x}_l)]$ so that it is possible to do imaging by removing the central parts of the cross correlations and migrating the tails. In backlight configurations such a separation and nulling is not possible with a single data set.

The use of differential cross correlations is natural in many applications in which we wish to image a local change in the medium, as when monitoring over time a volcano or an oil reservoir in geophysics, or tracking a moving target in the microwave regime. This is the reason that we use differential cross correlations exclusively in this paper.

2.4. Small decoherence time and correlation radius hypothesis

We assume that the decoherence time and the correlation radius of the noise sources are much smaller than the typical travel time and the typical travel distance that we want to estimate, that is, the travel time and distance from the localized reflectors to the sensor array. If we denote by ε the (small) ratio of these scales, then we can write the time correlation function F_ε and the local spatial covariance function H_ε of the noise sources in the form

$$F_\varepsilon(t_2 - t_1) = F\left(\frac{t_2 - t_1}{\varepsilon}\right), \quad H_\varepsilon(\mathbf{y}_2 - \mathbf{y}_1) = H\left(\frac{\mathbf{y}_2 - \mathbf{y}_1}{\varepsilon}\right), \quad (11)$$

where t_1 and t_2 are scaled relative to typical travel times and \mathbf{y}_1 and \mathbf{y}_2 are scaled relative to typical travel distances.

3. Structure of the cross correlations in a homogeneous medium

In this section we analyze the structure of the array cross correlations in the presence of localized reflectors. For this purpose we use the stationary phase method with ε as the small parameter for the asymptotic analysis. We assume that the background medium is homogeneous to simplify the presentation, although the results can be easily extended to the case of a smoothly varying background by using a geometrical optics approximation.

3.1. The background Green's function

For a homogeneous background with propagation speed c_0 , the time-harmonic Green's function \hat{G}_0 of the background medium is the solution of

$$\Delta_{\mathbf{x}} \hat{G}_0(\omega, \mathbf{x}, \mathbf{y}) + \frac{\omega^2}{c_0^2} \hat{G}_0(\omega, \mathbf{x}, \mathbf{y}) = -\delta(\mathbf{x} - \mathbf{y}), \quad (12)$$

along with a radiation condition at infinity. It is given by

$$\hat{G}_0(\omega, \mathbf{x}, \mathbf{y}) = \frac{1}{4\pi|\mathbf{x} - \mathbf{y}|} \exp(i\omega\mathcal{T}(\mathbf{x}, \mathbf{y})), \quad \mathcal{T}(\mathbf{x}, \mathbf{y}) = \frac{|\mathbf{x} - \mathbf{y}|}{c_0}. \quad (13)$$

Here $\mathcal{T}(\mathbf{x}, \mathbf{y})$ is the travel time from \mathbf{x} to \mathbf{y} . Substituting the expression (13) of the Green's function into (9), we obtain an expression of the theoretical cross correlation in the form of a multiple integral with a smooth amplitude function and a rapidly varying phase. The stationary phase method is therefore a natural tool for analyzing the structure of the cross correlation. As shown in [12], it is possible to analyze travel time estimation by cross correlation in order to identify the conditions under which the cross correlation has singular components at plus or minus the travel time between the sensors. The analysis can also be carried out in the presence of reflectors in the medium.

3.2. The peaks of the cross correlation in the presence of a reflector

We carry out the analysis when the background medium is homogeneous with propagation speed c_0 and there is a point reflector at \mathbf{z}_r . Since we assume that the reflector is weak and small, we can use the Born approximation for the Green's function (see Appendix A):

$$\hat{G}(\omega, \mathbf{x}, \mathbf{y}) = \hat{G}_0(\omega, \mathbf{x}, \mathbf{y}) + \frac{\omega^2}{c_0^2} \sigma_r l_r^3 \hat{G}_0(\omega, \mathbf{x}, \mathbf{z}_r) \hat{G}_0(\omega, \mathbf{z}_r, \mathbf{y}). \quad (14)$$

Here \hat{G}_0 is the Green's function (13) of the background medium, that is, in the absence of reflectors, σ_r is the reflectivity of the reflector, and l_r^3 is the volume of the reflector. The theoretical differential cross correlation is given by

$$\Delta C^{(1)}(\tau, \mathbf{x}_1, \mathbf{x}_2) = C^{(1)}(\tau, \mathbf{x}_1, \mathbf{x}_2) - C_0^{(1)}(\tau, \mathbf{x}_1, \mathbf{x}_2), \quad (15)$$

where $C^{(1)}$ is the theoretical cross correlation in the presence of the reflector (i.e. (9) with the full Green's function (14)) and $C_0^{(1)}$ is the theoretical cross correlation in the absence of the reflector (i.e. (9) with the background Green's function (12)). We collect the terms with the same power in $\sigma_r l_r^3$. The terms of order $O(1)$ cancel and we retain only the terms of order $O(\sigma_r l_r^3)$, consistent with the Born approximation:

$$\Delta C^{(1)}(\tau, \mathbf{x}_1, \mathbf{x}_2) = \Delta C_{\text{I}}^{(1)}(\tau, \mathbf{x}_1, \mathbf{x}_2) + \Delta C_{\text{II}}^{(1)}(\tau, \mathbf{x}_1, \mathbf{x}_2), \quad (16)$$

$$\begin{aligned} \Delta C_{\text{I}}^{(1)}(\tau, \mathbf{x}_1, \mathbf{x}_2) &= \frac{\sigma_r l_r^3 \varepsilon}{2\pi c_0^2} \iint d\mathbf{y} d\mathbf{z} d\omega K(\mathbf{y}) H(\mathbf{z}) \omega^2 \hat{F}(\omega) \overline{\hat{G}_0\left(\frac{\omega}{\varepsilon}, \mathbf{x}_1, \mathbf{z}_r\right)} \\ &\quad \times \overline{\hat{G}_0\left(\frac{\omega}{\varepsilon}, \mathbf{z}_r, \mathbf{y} + \frac{\varepsilon \mathbf{z}}{2}\right)} \hat{G}_0\left(\frac{\omega}{\varepsilon}, \mathbf{x}_2, \mathbf{y} - \frac{\varepsilon \mathbf{z}}{2}\right) \exp\left(-i\frac{\omega\tau}{\varepsilon}\right), \end{aligned} \quad (17)$$

$$\begin{aligned} \Delta C_{\text{II}}^{(1)}(\tau, \mathbf{x}_1, \mathbf{x}_2) &= \frac{\sigma_r l_r^3 \varepsilon}{2\pi c_0^2} \iint d\mathbf{y} d\mathbf{z} d\omega K(\mathbf{y}) H(\mathbf{z}) \omega^2 \hat{F}(\omega) \overline{\hat{G}_0\left(\frac{\omega}{\varepsilon}, \mathbf{x}_1, \mathbf{y} + \frac{\varepsilon \mathbf{z}}{2}\right)} \\ &\quad \times \hat{G}_0\left(\frac{\omega}{\varepsilon}, \mathbf{x}_2, \mathbf{z}_r\right) \overline{\hat{G}_0\left(\frac{\omega}{\varepsilon}, \mathbf{z}_r, \mathbf{y} - \frac{\varepsilon \mathbf{z}}{2}\right)} \exp\left(-i\frac{\omega\tau}{\varepsilon}\right). \end{aligned} \quad (18)$$

We see that the differential cross correlation technique removes the contributions of the direct waves so that the small singular components of the reflected waves can be observed better.

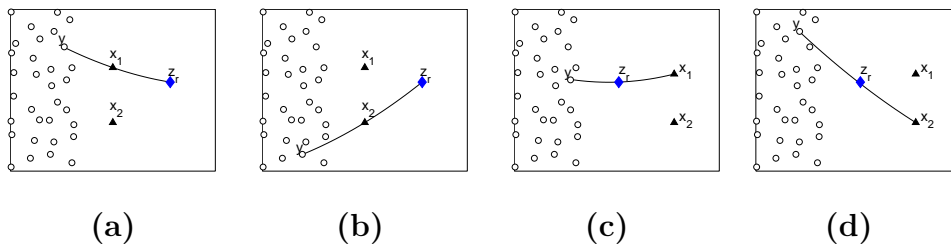


Figure 1. Different illumination configurations are plotted. The circles are noise sources, the triangles are sensors, and the diamond is the reflector. (a-b) are daylight configurations (the sensors are between the noise sources and the reflector), (c-d) are backlight configurations (the reflector is between the noise sources and the sensors).

The next propositions 3.1 and 3.2 are proved in Appendix B. They extend the qualitative result given in Proposition 6.1 in [12] in which the existence of the singular components of the differential cross correlation was obtained but their asymptotic forms were not computed. By identifying the existence of singular contributions at time lags equal to the sum or difference of travel times between sensors and reflectors, it becomes clear which is the appropriate migration imaging functional that should be used for the cross correlations, as we will see in Section 4.

The structure of the singular components depend on the illumination configuration. There are two main types of configurations of sources, sensors, and reflectors.

1) The noise sources are spatially localized and the sensors are between the sources and the reflectors (cases (a) and (b) in Figure 1). More precisely, the condition is that there are rays coming from the source region that go successively through a sensor and the reflector. We call this the daylight configuration. In such a configuration the singular components of the differential cross correlation are concentrated at (plus or minus) the sum of travel times $\mathcal{T}(\mathbf{x}_2, \mathbf{z}_r) + \mathcal{T}(\mathbf{x}_1, \mathbf{z}_r)$.

2) The noise sources are spatially localized and the reflectors are between the sources and the sensors (cases (c) and (d) in Figure 1). More precisely, the condition is that there are rays coming from the source region that go successively through the reflector and a sensor. As in [12], we call this the backlight configuration, by analogy with photography. In a backlight configuration the singular components of the differential cross correlation are concentrated at the difference of travel times $\mathcal{T}(\mathbf{x}_2, \mathbf{z}_r) - \mathcal{T}(\mathbf{x}_1, \mathbf{z}_r)$.

An arbitrary noise source configuration may provide either daylight or backlight illumination, or none of them, or both of them. When the source configuration provide both (resp. none) daylight and backlight illuminations, then the differential cross correlation has both (resp. none) singular components described in the next two propositions.

Proposition 3.1 *In the backlight illumination configuration, in the asymptotic regime $\varepsilon \rightarrow 0$, the differential cross correlation has a unique singular contribution centered at*

the difference of travel times $\mathcal{T}(\mathbf{x}_2, \mathbf{z}_r) - \mathcal{T}(\mathbf{x}_1, \mathbf{z}_r)$ and it has the form:

$$\Delta C^{(1)}(\tau, \mathbf{x}_1, \mathbf{x}_2) \approx \frac{\sigma_r l_r^3 \varepsilon^3}{32\pi^2 c_0} \frac{K_{\mathbf{z}_r, \mathbf{x}_2} - K_{\mathbf{z}_r, \mathbf{x}_1}}{|\mathbf{z}_r - \mathbf{x}_1| |\mathbf{z}_r - \mathbf{x}_2|} \partial_\tau F_H \left(\frac{\tau - [\mathcal{T}(\mathbf{x}_2, \mathbf{z}_r) - \mathcal{T}(\mathbf{x}_1, \mathbf{z}_r)]}{\varepsilon} \right), \quad (19)$$

where

$$K_{\mathbf{z}, \mathbf{x}} = \int_0^\infty K \left(\mathbf{z} + \frac{\mathbf{z} - \mathbf{x}}{|\mathbf{z} - \mathbf{x}|} l \right) dl, \quad \hat{F}_H(\omega) = \hat{F}(\omega) \hat{H} \left(\frac{\omega}{c_0} \right). \quad (20)$$

The coefficient $K_{\mathbf{z}_r, \mathbf{x}_j}$ is the energy flux that contributes to the peak centered at the difference of the travel times. This coefficient is zero unless the ray going from \mathbf{x}_j to \mathbf{z}_r extends into the source region, which is the support of the function K . Therefore, a peak at the difference of travel times appears only in the backlight illumination configuration.

Proposition 3.2 *In the daylight illumination configuration, the differential cross correlation has two singular contributions which are centered at plus or minus the sum of the travel times $\mathcal{T}(\mathbf{x}_1, \mathbf{z}_r) + \mathcal{T}(\mathbf{x}_2, \mathbf{z}_r)$. The peak centered at plus the sum of travel times has the form:*

$$\Delta C^{(1)}(\tau, \mathbf{x}_1, \mathbf{x}_2) \approx \frac{\sigma_r l_r^3 \varepsilon^3}{32\pi^2 c_0} \frac{K_{\mathbf{x}_1, \mathbf{z}_r}}{|\mathbf{z}_r - \mathbf{x}_1| |\mathbf{z}_r - \mathbf{x}_2|} \partial_\tau F_H \left(\frac{\tau - [\mathcal{T}(\mathbf{x}_2, \mathbf{z}_r) + \mathcal{T}(\mathbf{x}_1, \mathbf{z}_r)]}{\varepsilon} \right). \quad (21)$$

The peak centered at minus the sum of travel times has the form:

$$\Delta C^{(1)}(\tau, \mathbf{x}_1, \mathbf{x}_2) \approx -\frac{\sigma_r l_r^3 \varepsilon^3}{32\pi^2 c_0} \frac{K_{\mathbf{x}_2, \mathbf{z}_r}}{|\mathbf{z}_r - \mathbf{x}_1| |\mathbf{z}_r - \mathbf{x}_2|} \partial_\tau F_H \left(\frac{\tau + [\mathcal{T}(\mathbf{x}_2, \mathbf{z}_r) + \mathcal{T}(\mathbf{x}_1, \mathbf{z}_r)]}{\varepsilon} \right). \quad (22)$$

The coefficient $K_{\mathbf{x}_j, \mathbf{z}_r}$ is the energy flux that contributes to the peak centered at plus or minus the sum of travel times. Note that $K_{\mathbf{x}_j, \mathbf{z}_r}$ is zero unless the ray going from \mathbf{z}_r to \mathbf{x}_j extends into the source region. That is why the peaks at plus or minus the sum of travel times appear only in the daylight illumination configuration.

The width of the singular peak at the sum or difference of travel times is equal to the width of the function F_H , measured in some manner such as the normalized standard deviation. The function F_H is the convolution of the time correlation function and the spatial covariance function of the noise sources. Let us denote by τ_c the time coherence of the noise sources, which is the reciprocal of the bandwidth B , and by ρ_c the correlation radius. The width T_s of the function F_H is of the order of the sum of τ_c and ρ_c/c_0 . If, for example, the functions F and H are Gaussian, then we have

$$T_s^2 = \tau_c^2 + \frac{\rho_c^2}{c_0^2}. \quad (23)$$

4. Resolution analysis of correlation based imaging

4.1. The daylight imaging functional

First, we consider migration imaging with daylight illumination. The imaging functional at a search point \mathbf{z}^S is the *daylight migration imaging functional*

$$\begin{aligned} \mathcal{I}^D(\mathbf{z}^S) = & \frac{1}{2} \sum_{j,l=1}^N \Delta C(\mathcal{T}(\mathbf{z}^S, \mathbf{x}_l) + \mathcal{T}(\mathbf{z}^S, \mathbf{x}_j), \mathbf{x}_j, \mathbf{x}_l) \\ & + \Delta C(-\mathcal{T}(\mathbf{z}^S, \mathbf{x}_l) - \mathcal{T}(\mathbf{z}^S, \mathbf{x}_j), \mathbf{x}_j, \mathbf{x}_l). \end{aligned} \quad (24)$$

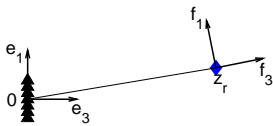


Figure 2. The two reference frames (\hat{e}_1, \hat{e}_3) (associated with the sensor array) and (\hat{f}_1, \hat{f}_3) (defining the transverse and longitudinal directions for the imaging functional). The unit vectors $\hat{e}_2 = \hat{f}_2$ are orthogonal to the plane of the figure.

Since the cross correlation satisfies $C(-\tau, \mathbf{x}_j, \mathbf{x}_l) = C(\tau, \mathbf{x}_l, \mathbf{x}_j)$, the second sum is equal to the first one. It is a consequence of Proposition 3.1 that the migration should be done with (plus or minus) the sum of travel times $\mathcal{T}(\mathbf{z}^S, \mathbf{x}_l) + \mathcal{T}(\mathbf{z}^S, \mathbf{x}_j)$. It is shown in the proposition that the singular component of $\Delta C(\tau, \mathbf{x}_j, \mathbf{x}_l)$ is at $\tau = \pm[\mathcal{T}(\mathbf{z}_r, \mathbf{x}_l) + \mathcal{T}(\mathbf{z}_r, \mathbf{x}_j)]$. The resolution of the daylight imaging functional is comparable to that of the Kirchhoff migration (KM) functional used in active sensor imaging when a localized reflector is illuminated by active sensors at $(\mathbf{x}_j)_{j=1, \dots, N}$ [4]. Indeed, in active sensor imaging the sensor at \mathbf{x}_l emits an impulse, the sensor at \mathbf{x}_j records the signal $P(t, \mathbf{x}_j, \mathbf{x}_l)$, and the KM imaging functional is then

$$\mathcal{I}^{\text{KM}}(\mathbf{z}^S) = \sum_{j,l=1}^N P(\mathcal{T}(\mathbf{z}^S, \mathbf{x}_j) + \mathcal{T}(\mathbf{z}^S, \mathbf{x}_l), \mathbf{x}_j, \mathbf{x}_l),$$

which involves the sum of travel times as in the daylight imaging functional (24).

In order to analyze the resolution properties of the daylight imaging functional, we first introduce a coordinate frame $(\hat{e}_1, \hat{e}_2, \hat{e}_3)$ such that (see Figure 2):

- 1) the planar array is centered at $\mathbf{0}$ and occupies a region A in the plane (\hat{e}_1, \hat{e}_2) ,
- 2) the reflector is in the plane (\hat{e}_1, \hat{e}_3) with coordinates $\mathbf{z}_r = (x_r, 0, z_r)$.

We also introduce the orthonormal frame $(\hat{f}_1, \hat{f}_2, \hat{f}_3)$ where

$$\hat{f}_1 = \frac{1}{|\mathbf{z}_r|}(z_r \hat{e}_1 - x_r \hat{e}_3), \quad \hat{f}_2 = \hat{e}_2, \quad \hat{f}_3 = \frac{\mathbf{z}_r}{|\mathbf{z}_r|} = \frac{1}{|\mathbf{z}_r|}(x_r \hat{e}_1 + z_r \hat{e}_3). \quad (25)$$

The vectors (\hat{f}_1, \hat{f}_2) define the transverse directions and the vector \hat{f}_3 defines the longitudinal direction. The resolution of the image will depend on the tilt of the array relative to \hat{f}_3 . It is therefore convenient to introduce the cosine of the tilt angle

$$\alpha_r = \hat{f}_3 \cdot \hat{e}_3 = \frac{z_r}{|\mathbf{z}_r|}. \quad (26)$$

To quantify the imaging resolution we compute the point spread function, which is the spatial profile of the imaging functional centered at a point reflector. The cross range resolution and the range resolution are the widths of the point spread function in the transverse and longitudinal directions, respectively. They depend on the characteristic scales of the problem: the typical diameter a of the sensor array, the distance $|\mathbf{z}_r|$ from the center of the sensor array to the point reflector, the typical wavelength λ_0 , and the

bandwidth $1/T_s$, T_s is the time width (23) of the peaks of the cross correlation. We assume that the typical wavelength λ_0 of the noise sources is smaller than the diameter a of the sensor array which is smaller than the distance $|\mathbf{z}_r|$ from the array to the reflector.

We introduce the normalized shape A_0 of the sensor array such that $A = aA_0$ and we define the normalized, narrowband point spread function by

$$\mathcal{G}_{\alpha_r}(\eta_1, \eta_2, \eta_3) = \frac{1}{|A_0|} \int_{A_0} \exp \left[-i(\alpha_r u_1 \eta_1 + u_2 \eta_2) - i \frac{u_1^2 \alpha_r^2 + u_2^2}{2} \eta_3 \right] du_1 du_2. \quad (27)$$

Proposition 4.1 *The daylight imaging functional at the search point \mathbf{z}^S ,*

$$\mathbf{z}^S = \mathbf{z}_r + \boldsymbol{\xi}^S = \mathbf{z}_r + \xi_1 \hat{\mathbf{f}}_1 + \xi_2 \hat{\mathbf{f}}_2 + \xi_3 \hat{\mathbf{f}}_3,$$

such that $|\boldsymbol{\xi}^S| \ll |\mathbf{z}_r|$, has the asymptotic form

$$\mathcal{I}^D(\mathbf{z}^S) \approx \mathcal{I}^D(\mathbf{z}_r) \mathcal{P}^D(\boldsymbol{\xi}^S),$$

where $\mathcal{I}^D(\mathbf{z}_r)$ is the peak amplitude

$$\mathcal{I}^D(\mathbf{z}_r) = \frac{N^2 \sigma_r l_r^3 \varepsilon^3 K_{\mathbf{0}, \mathbf{z}_r}}{64 \pi^3 c_0 |\mathbf{z}_r|^2},$$

and $\mathcal{P}^D(\boldsymbol{\xi}^S)$ is the point spread function

$$\mathcal{P}^D(\boldsymbol{\xi}^S) = \int d\omega i\omega \hat{F}_H(\omega) \exp \left[i \frac{\omega}{c_0} (2\xi_3 + \frac{\xi_1^2 + \xi_2^2}{|\mathbf{z}_r|}) \right] \mathcal{G}_{\alpha_r} \left(\frac{\omega a}{c_0 |\mathbf{z}_r|} \xi_1, \frac{\omega a}{c_0 |\mathbf{z}_r|} \xi_2, \frac{\omega a^2}{c_0 |\mathbf{z}_r|^2} \xi_3 \right)^2. \quad (28)$$

The expression (28) of the point spread function follows from a stationary phase analysis of the daylight imaging functional in the continuum approximation of a dense array (see Appendix C). In particular the form (28) of the point spread function shows that the longitudinal coordinate ξ_3 appears both as an argument in the normalized function \mathcal{G}_{α_r} and in the inverse Fourier transform of $\hat{F}_H(\omega)$. As a result there is a competition between these two terms to determine the range resolution, and the result depends on whether the effective bandwidth $B = 1/T_s$ of \hat{F}_H is smaller or larger than a threshold value, as described in the next proposition.

Proposition 4.2 *Let us assume that the Fourier transform of F_H has the form*

$$\hat{F}_H(\omega) = \frac{1}{2B} \left[\hat{F}_{H,0} \left(\frac{\omega_0 - \omega}{B} \right) + \hat{F}_{H,0} \left(\frac{\omega_0 + \omega}{B} \right) \right], \quad (29)$$

where ω_0 is the central frequency and B is the bandwidth (i.e. $B = 1/T_s$).

If the bandwidth B of \hat{F}_H is smaller than its central frequency ω_0 but larger than the critical value

$$B_c = \frac{\omega_0 a^2}{2 |\mathbf{z}_r|^2}, \quad (30)$$

then the slowly varying envelope of the point spread function has the form

$$\mathcal{P}^D(\boldsymbol{\xi}^S) \approx \pi \omega_0 \left| \mathcal{G}_{\alpha_r} \left(\frac{\omega_0 a}{c_0 |\mathbf{z}_r|} \xi_1, \frac{\omega_0 a}{c_0 |\mathbf{z}_r|} \xi_2, 0 \right) \right|^2 \left| F_{H,0} \left(\frac{2B\xi_3}{c_0} + \frac{B(\xi_1^2 + \xi_2^2)}{c_0 |\mathbf{z}_r|} \right) \right|. \quad (31)$$

If the bandwidth B of \hat{F}_H is smaller than the critical value B_c , then the slowly varying envelope of the point spread function is

$$\mathcal{P}^D(\boldsymbol{\xi}^S) \approx \pi\omega_0 \left| \mathcal{G}_{\alpha_r} \left(\frac{\omega_0 a}{c_0 |\mathbf{z}_r|} \xi_1, \frac{\omega_0 a}{c_0 |\mathbf{z}_r|} \xi_2, \frac{\omega_0 a^2}{c_0 |\mathbf{z}_r|^2} \xi_3 \right) \right|^2 |F_{H,0}(0)|. \quad (32)$$

The central wavelength is given by $\lambda_0 = 2\pi c_0 / \omega_0$. We see from (31) and (32) that the scale factors in the arguments of the point spread functions can be expressed in terms of the central wavelength. We define cross range and range resolutions in terms of the width of the point spread functions, which involves the scale factors as follows.

In both the broadband case (31) and in the narrowband case (32) the cross range resolution is

- $\lambda_0 |\mathbf{z}_r| / (a\alpha_r)$ in the $\hat{\mathbf{f}}_1$ -direction,
- $\lambda_0 |\mathbf{z}_r| / a$ in the $\hat{\mathbf{f}}_2$ -direction.

In the broadband case (31) the range resolution is

- $c_0 / (2B)$ in the $\hat{\mathbf{f}}_3$ -direction.

In the narrowband case (32) the range resolution is

- $\lambda_0 |\mathbf{z}_r|^2 / a^2$ in the $\hat{\mathbf{f}}_3$ -direction.

This way of defining cross range and range resolution is consistent with, and a generalization of, the classical definition of resolution introduced by Rayleigh [5]. To see this we note that the point spread function depends on the shape of the sensor array (see Figure 3). For simplicity we consider a point reflector in the axis of the sensor array, with no tilt $x_r = 0$.

1) The function

$$\mathcal{G}_1(\eta_1, \eta_2, 0) = \frac{1}{|A_0|} \int_{A_0} \exp \left[-i(u_1 \eta_1 + u_2 \eta_2) \right] du_1 du_2$$

is the normalized point spread function in the transverse plane, along the cross range directions. It is proportional to the Fourier transform of the normalized support function $\mathbf{1}_{A_0}$ of the array. Since the support function takes only values 0 and 1 and is not continuous, the decay rate at infinity of the function \mathcal{G}_1 is a power law.

2) The normalized point spread function in the longitudinal axis, which is the range direction, is given by

$$\mathcal{G}_1(0, 0, \eta_3) = \frac{1}{|A_0|} \int_{A_0} \exp \left[-i \frac{u_1^2 + u_2^2}{2} \eta_3 \right] du_1 du_2$$

for narrowband noise sources, and $|F_{H,0}(-\eta_3)|$ for broadband noise sources.

We can describe more explicitly the normalized point spread function in two special cases.

1) If the array is a disk with diameter a , then the spatial profile of the normalized point spread function in the transverse directions is the Airy distribution

$$\mathcal{G}_1(\eta_1, \eta_2, 0) = 2 \frac{J_1(\sqrt{\eta_1^2 + \eta_2^2}/2)}{\sqrt{\eta_1^2 + \eta_2^2}/2},$$

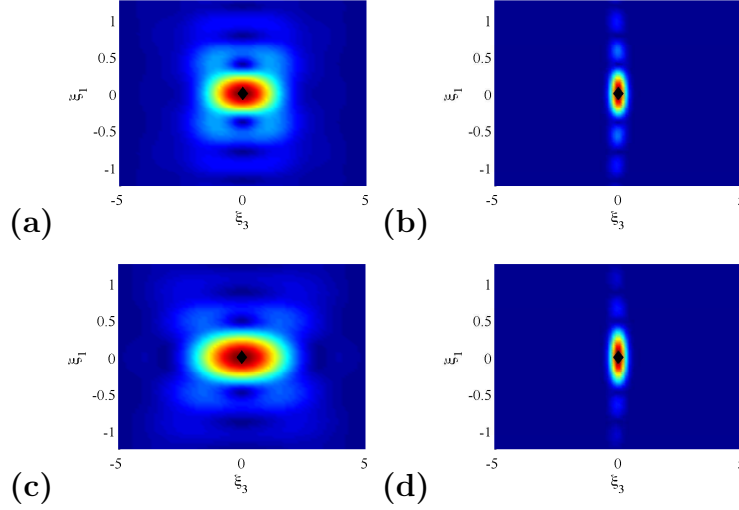


Figure 3. The slowly varying envelope of the point spread function $\mathcal{P}^D(\xi_1, 0, \xi_3)$ of the daylight imaging functional in the transverse direction $\hat{\mathbf{f}}_1$ (with coordinate ξ_1) and in the longitudinal direction $\hat{\mathbf{f}}_3$ (with coordinate ξ_3). Here the reflector $\mathbf{z}_r = (0, 0, 100)$ is localized on the axis of the sensor array whose diameter is $a = 10$ and the noise spectrum is Gaussian $F_H(t) = \exp(-B^2 t^2) \cos(\omega_0 t)$ with the central frequency $\omega_0 = 2\pi$ and the central wavelength $\lambda_0 = 1$ (the background velocity is $c_0 = 1$). The critical bandwidth (30) is $B_c \simeq 0.03$. (a): narrowband noise sources $B = 0.01$ and a square sensor array with side length $a = 10$; (b): narrowband noise sources $B = 0.01$ and a square sensor array with side length $a = 10$; (c): broadband noise sources $B = 0.1$ and a disk sensor array with diameter $a = 10$; (d): broadband noise sources $B = 0.1$ and a disk sensor array with diameter $a = 10$.

and in the longitudinal direction it is

$$\mathcal{G}_1(0, 0, \eta_3) = \frac{8}{\eta_3} \left[\sin \frac{\eta_3}{8} - i(1 - \cos \frac{\eta_3}{8}) \right], \quad |\mathcal{G}_1(0, 0, \eta_3)| = \left| \frac{\sin(\eta_3/16)}{\eta_3/16} \right|.$$

Here J_1 is the Bessel function of order one. The first zero of the Airy distribution is at $\sqrt{\eta_1^2 + \eta_2^2} \simeq 7.66$. In dimensional coordinates this corresponds to $\sqrt{\xi_1^2 + \xi_2^2} \simeq 1.22\lambda_0|\mathbf{z}_r|/a$, which is a result obtained originally by Lord Rayleigh in his investigation of the limit of resolution of optical instruments [5].

2) If the array is a square with side length a , then the spatial profile of the normalized point spread function in the transverse directions is the sinc distribution

$$\mathcal{G}_1(\eta_1, \eta_2, 0) = \frac{\sin(\eta_1/2)}{\eta_1/2} \frac{\sin(\eta_2/2)}{\eta_2/2},$$

and in the longitudinal direction it is

$$\mathcal{G}_1(0, 0, \eta_3) = \frac{4\pi}{\eta_3} (C - iS)^2 \left(\frac{\sqrt{\eta_3}}{2\sqrt{\pi}} \right), \quad |\mathcal{G}_1(0, 0, \eta_3)| = \frac{4\pi}{\eta_3} (C^2 + S^2) \left(\frac{\sqrt{\eta_3}}{2\sqrt{\pi}} \right),$$

where C and S are the Fresnel integrals

$$C(u) = \int_0^u \cos\left(\frac{\pi s^2}{2}\right) ds, \quad S(u) = \int_0^u \sin\left(\frac{\pi s^2}{2}\right) ds.$$

To summarize, the daylight imaging functional has the following resolution properties.

1) When there is no tilt ($\alpha_r = 1$ in (26)), the cross range resolution of the daylight imaging functional is given by

$$\frac{\lambda_0 |\mathbf{z}_r|}{a}. \quad (33)$$

This is the classical Rayleigh resolution formula for active array imaging [5, 4]. When there is tilt then, in the direction of the tilt, the cross range resolution is given by the Rayleigh formula with a replaced by the effective diameter $a\alpha_r$.

2) The range resolution for broadband noise sources is $c_0 T_s / 2$. For narrowband noise sources the range resolution is $\lambda_0 |\mathbf{z}_r|^2 / a^2$.

From these results we see that the cross range and range resolution formulas for daylight noise imaging are the same as those for active array imaging with the effective bandwidth $1/T_s$.

4.2. The backlight imaging functional

We now consider migration imaging with backlight illumination. The imaging functional at a search point \mathbf{z}^S is the *backlight imaging functional*

$$\mathcal{I}^B(\mathbf{z}^S) = \sum_{j,l=1}^N \Delta C(\mathcal{T}(\mathbf{z}^S, \mathbf{x}_l) - \mathcal{T}(\mathbf{z}^S, \mathbf{x}_j), \mathbf{x}_j, \mathbf{x}_l). \quad (34)$$

The sign of the travel time in the argument of the imaging functional is determined by Proposition 3.2. It is shown there that the peak of $\Delta C(\tau, \mathbf{x}_j, \mathbf{x}_l)$ is at $\tau = \mathcal{T}(\mathbf{z}_r, \mathbf{x}_l) - \mathcal{T}(\mathbf{z}_r, \mathbf{x}_j)$.

The form of the backlight imaging functional is similar to the incoherent interferometric imaging functional. This imaging functional is used when \mathbf{z}_r is a source emitting an incoherent signal that is recorded by passive sensors at $(\mathbf{x}_j)_{j=1,\dots,N}$ and the data is the vector $(P(t, \mathbf{x}_j)_{j=1,\dots,N,t \in \mathbb{R}})$ [4]. The incoherent interferometric functional (IINT) has the form

$$\begin{aligned} \mathcal{I}^{\text{IINT}}(\mathbf{z}^S) &= \frac{1}{2\pi} \int d\omega \left| \sum_{l=1}^N \exp(-i\omega \mathcal{T}(\mathbf{z}^S, \mathbf{x}_l)) \hat{P}(\omega, \mathbf{x}_l) \right|^2 \\ &= \frac{1}{2\pi} \int d\omega \sum_{j,l=1}^N \exp(-i\omega [\mathcal{T}(\mathbf{z}^S, \mathbf{x}_l) - \mathcal{T}(\mathbf{z}^S, \mathbf{x}_j)]) \hat{P}(\omega, \mathbf{x}_l) \overline{\hat{P}(\omega, \mathbf{x}_j)}, \end{aligned}$$

which is a matched field imaging functional. It involves a difference of travel times as does the backlight imaging functional (34), which in the Fourier domain is given by

$$\mathcal{I}^B(\mathbf{z}^S) = \frac{1}{2\pi} \int d\omega \sum_{j,l=1}^N \exp(-i\omega [\mathcal{T}(\mathbf{z}^S, \mathbf{x}_l) - \mathcal{T}(\mathbf{z}^S, \mathbf{x}_j)]) \widehat{\Delta C}(\omega, \mathbf{x}_j, \mathbf{x}_l).$$

The resolution of the backlight imaging functional is obtained from the next proposition.

Proposition 4.3 *We use the same notation as for the daylight imaging functional in the previous subsection.*

The backlight imaging functional at a search point $\mathbf{z}^S = \mathbf{z}_r + \boldsymbol{\xi}^S$ around the reflector location \mathbf{z}_r has the form

$$\begin{aligned} \mathcal{I}^B(\mathbf{z}^S) \approx & -\frac{\sigma_r l_r^3 N^2}{2^4 \pi^3 |\mathbf{z}_r|} \int d\omega \hat{F}_H(\omega) \\ & \times \left[\frac{|\mathbf{z}_r|}{z_r} \partial_{x_1} K_{\mathbf{z}_r, \mathbf{0}} \partial_{\xi_1} + \partial_{x_2} K_{\mathbf{z}_r, \mathbf{0}} \partial_{\xi_2} \right] \left| \mathcal{G}_{\alpha_r} \left(\frac{\omega a}{c_0 |\mathbf{z}_r|} \xi_1, \frac{\omega a}{c_0 |\mathbf{z}_r|} \xi_2, \frac{\omega a^2}{c_0 |\mathbf{z}_r|^2} \xi_3 \right) \right|^2. \end{aligned} \quad (35)$$

If the function F_H has the form (29) and if the bandwidth B of \hat{F}_H is smaller than its central frequency ω_0 then the slowly varying envelope of the backlight imaging functional is approximately

$$\begin{aligned} \mathcal{I}^B(\mathbf{z}^S) \approx & \frac{\sigma_r l_r^3 N^2}{2^3 \pi^2 |\mathbf{z}_r|} |F_{H,0}(0)| \\ & \times \left[\frac{|\mathbf{z}_r|}{z_r} \partial_{x_1} K_{\mathbf{z}_r, \mathbf{0}} \partial_{\xi_1} + \partial_{x_2} K_{\mathbf{z}_r, \mathbf{0}} \partial_{\xi_2} \right] \left| \mathcal{G}_{\alpha_r} \left(\frac{\omega_0 a}{c_0 |\mathbf{z}_r|} \xi_1, \frac{\omega_0 a}{c_0 |\mathbf{z}_r|} \xi_2, \frac{\omega_0 a^2}{c_0 |\mathbf{z}_r|^2} \xi_3 \right) \right|^2. \end{aligned} \quad (36)$$

To summarize, the resolution of the backlight imaging functional is as follows.

- 1) The cross range resolution is the same as that of the daylight imaging functional and is given by the Rayleigh resolution formula (33).
- 2) The range resolution is given by $\lambda_0 |\mathbf{z}_r|^2 / a^2$, even for broadband noise sources.

Compared to the daylight imaging functional the backlight imaging functional has poor range resolution because it is based on a difference of travel times, which is less sensitive to the range than the sum of travel times used in the daylight imaging functional.

The backlight imaging functional uses the peak of the cross correlations at the difference of travel times (19). The amplitude of cross correlations at this peak is proportional to $K_{\mathbf{z}_r, \mathbf{x}_l} - K_{\mathbf{z}_r, \mathbf{x}_j}$, which can change sign. This is in contrast with the daylight imaging functional where the amplitudes of the cross correlations (21) at the sum travel times have a well-defined sign. As a result the daylight imaging functional is more stable with respect to the spatial support of the noise sources than the backlight imaging functional.

4.3. Numerical simulations

We present numerical simulations in which we calculate the theoretical cross correlations $C^{(1)}$ and $C_0^{(1)}$ for different configurations of noise sources, reflectors, and sensors. The theoretical cross correlation is what is obtained with the empirical cross correlation C_T in the limit of an infinitely large integration time T . The statistical stability (i.e. the decay of the fluctuations of C_T with respect to its statistical average for large T) has been studied in detail theoretically and numerically in [12]. It is not a limiting factor in this type of problems as long as the recording time window is sufficiently large.

We consider a homogeneous background medium with velocity $c_0 = 1$. We compute the image in the plane (x, z) and use the homogeneous background Green's function (13).

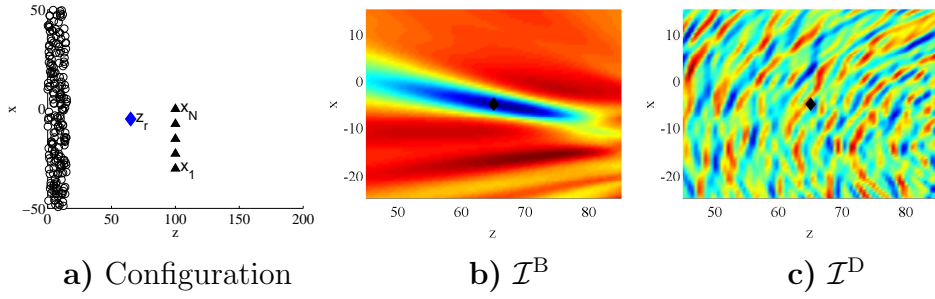


Figure 4. Passive sensor imaging using the differential cross correlation technique in a homogeneous medium. The backlight illumination configuration is plotted in Figure a: the circles are the noise sources, the triangles are the sensors, and the diamond is the reflector. Figure b plots the image obtained with the backlight imaging functional (34). Figure c plots the image obtained with the daylight imaging functional (24).

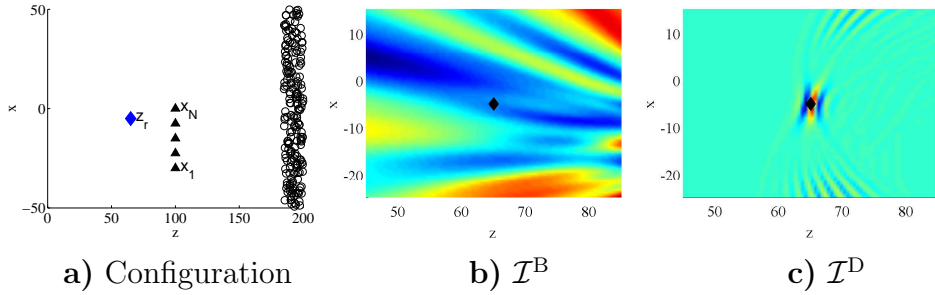


Figure 5. Passive sensor imaging using the differential cross correlation technique in a homogeneous medium. The daylight illumination configuration is plotted in Figure a: the circles are the noise sources, the triangles are the sensors, and the diamond is the reflector. Figure b plots the image obtained with the backlight imaging functional (34). Figure c plots the image obtained with the daylight imaging functional (24).

The random sources are a collection of 100 randomly located point sources in a layer of size 100×15 with power spectral density $\hat{F}(\omega) = \omega^2 \exp(-\omega^2)$. We consider a point reflector at position $(-5, 60)$ with $\sigma_r I_r^3 = 0.01$ and a linear array of 5 sensors located at $(-37.5 + 7.5j, 100)$, $j = 1, \dots, 5$. The central wavelength is therefore $\lambda_0 \simeq 6$, the diameter of the array is $a = 30$, and the distance from the sensor array to the reflector is $|z_r| \simeq 40$. The expected theoretical cross-range resolution is, therefore, about 8, the range resolution for the daylight imaging functional is about 2, and the range resolution for the backlight imaging functional is about 40.

In Figure 4 we consider a backlight illumination configuration. We apply both the backlight imaging functional (34) and the daylight imaging functional (24). As predicted by the theory, the backlight imaging functional gives a good cross range resolution of the target but a very poor range resolution. The daylight imaging functional is not efficient.

In Figure 5 we consider a daylight illumination configuration. As predicted by the theory, the daylight imaging functional gives good cross range and range resolutions of

the target. The backlight imaging functional is not efficient.

4.4. Role of illumination diversity

In this paper we have analyzed configurations that provide either daylight or backlight illuminations. In practice we usually encounter illumination configurations that are not purely daylight or backlight.

Favorable illumination situations arise when the noise sources are distributed around the sensors and the reflectors so as to provide both daylight and backlight illuminations. The imaging functionals (24) and (34) can then provide images of the region around the reflectors with the same resolution properties as separately for daylight and backlight illuminations. Therefore both imaging functionals can be used to enhance the signal-to-noise ratio. However the daylight imaging functional (24) has a much better range resolution than (34) and so it should be preferred, if possible.

Unfavorable illumination situations arise when the noise sources are distributed so as to provide neither daylight nor backlight illumination. Both imaging functionals then give poor images. When the background medium is not homogeneous and there is scattering, it is possible to exploit this scattering to enhance the directional diversity of the overall illumination. In that case the scatterers act as secondary noise sources [22, 12] but scattering will also tend to blur the images [9, 13].

5. Summary and conclusions

We have analyzed the resolution properties of the daylight and backlight imaging functionals (24) and (34), respectively, which can be used to image reflectors in a medium illuminated by ambient noise sources. In Propositions 4.2 and 4.3 we obtain integral formulas that allow us to describe quantitatively the cross range and range resolutions of the two imaging functionals. We have shown that the cross range resolution is given by the classical Rayleigh resolution formula (33) for both functionals. We have also shown that the range resolution of the daylight imaging functional is the same as that for active array imaging for both narrowband and broadband noise sources. However, the backlight imaging functional has poor range resolution regardless of the bandwidth because it uses the difference of travel times between sensors and reflectors while the daylight imaging functional uses the sum of travel times. The analysis shows that the effective bandwidth of the noise sources for imaging is determined by the time and space correlations of the noise sources (23). In the case of spatially uncorrelated noise sources the bandwidth is the inverse of the coherence time of the noise sources. In the case of spatially correlated sources the bandwidth is smaller than the inverse of the coherence time and the range resolution (for the daylight imaging functional) is reduced.

It is therefore preferable to use the daylight imaging functional, which requires a daylight illumination of the reflector. When only backlight illumination is available, it is possible to exploit the scattering properties of the medium and the enhanced directional

diversity of the scattered waves to generate an effective daylight illumination [11]. Imaging with this type of daylight illumination requires, however, a detailed analysis of the trade-off between the enhanced directional diversity of the scattered waves and the reduction in the signal-to-noise ratio for the peaks of the cross correlation at the sum and difference of travel times.

Acknowledgments

This work was supported in part by US Army grant W911NF-07-2-0027-1 and by AFOSR grant FA9550-08-1-0089.

Appendix A. The Born approximation for a point scatterer

We describe briefly the Born approximation for the point scatterer introduced in Subsection 3.2 to calculate the cross correlation in the presence of a reflector. We assume that the medium is homogeneous with background velocity c_0 . A localized scatterer around \mathbf{z}_r is modeled by a local variation $V_r(\mathbf{x})$ of the speed of propagation:

$$\frac{1}{c^2(\mathbf{x})} = \frac{1}{c_0^2}(1 + \sigma_r V_r(\mathbf{x})), \quad V_r(\mathbf{x}) = \mathbf{1}_{\Omega_r}(\mathbf{x} - \mathbf{z}_r).$$

Here Ω_r is a compactly supported domain with volume l_r^3 . The solution of the full wave equation can be written in the Fourier domain as the sum

$$\hat{u}(\omega, \mathbf{x}) = \hat{u}_0(\omega, \mathbf{x}) + \hat{u}_1(\omega, \mathbf{x}),$$

where the direct field u_0 satisfies the wave equation (1) with the background velocity c_0 and it is given by:

$$\hat{u}_0(\omega, \mathbf{x}) = \int \hat{G}_0(\omega, \mathbf{x}, \mathbf{y}) \hat{n}(\omega, \mathbf{y}) d\mathbf{y}, \quad (\text{A.1})$$

with \hat{G}_0 the time-harmonic Green's function of the background medium (13). The scattered field u_1 is solution of the homogeneous wave equation with the source term $-c_0^{-2} V_r(\mathbf{x}) \partial_t^2 u(t, \mathbf{x})$, so that it is given in the Fourier domain by

$$\hat{u}_1(\omega, \mathbf{x}) = \frac{\omega^2}{c_0^2} \int \hat{G}_0(\omega, \mathbf{x}, \mathbf{z}) V_r(\mathbf{z}) \hat{u}(\omega, \mathbf{z}) d\mathbf{z}. \quad (\text{A.2})$$

This expression is exact. The Born approximation (or single-scattering approximation) consists in replacing \hat{u} on the right side of (A.2) by the field \hat{u}_0 , which gives [5]:

$$\hat{u}_1(\omega, \mathbf{x}) \simeq \frac{\omega^2}{c_0^2} \iint \hat{G}_0(\omega, \mathbf{x}, \mathbf{z}) V_r(\mathbf{z}) \hat{G}_0(\omega, \mathbf{z}, \mathbf{y}) \hat{n}(\omega, \mathbf{y}) d\mathbf{z} d\mathbf{y}.$$

This approximation is valid if the scattered field u_1 is small compared to the incident field u_0 . We also assume that the diameter l_r of the scattering region Ω_r is small compared to typical wavelength. We can then model the scatterer by a point scatterer:

$$\mathbf{1}_{\Omega_r}(\mathbf{x} - \mathbf{z}_r) \approx \sigma_r l_r^3 \delta(\mathbf{x} - \mathbf{z}_r),$$

and we can write the scattered field u_1 in the form

$$\hat{u}_1(\omega, \mathbf{x}) = \frac{\omega^2}{c_0^2} \sigma_r l_r^3 \int \hat{G}_0(\omega, \mathbf{x}, \mathbf{z}_r) \hat{G}_0(\omega, \mathbf{z}_r, \mathbf{y}) \hat{n}(\omega, \mathbf{y}) d\mathbf{y}. \quad (\text{A.3})$$

This shows that the full Green's function can be written as $\hat{G} = \hat{G}_0 + \hat{G}_1$ in the Born approximation with \hat{G}_1 given by

$$\hat{G}_1(\omega, \mathbf{x}, \mathbf{y}) = \frac{\omega^2}{c_0^2} \sigma_r l_r^3 \hat{G}_0(\omega, \mathbf{x}, \mathbf{z}_r) \hat{G}_0(\omega, \mathbf{z}_r, \mathbf{y}). \quad (\text{A.4})$$

Appendix B. Proof of Proposition 3.1

We consider the backlight illumination configuration and first focus our attention to the term $\Delta C_I^{(1)}$. By a Taylor series expansion we obtain

$$\left| \mathbf{x}_2 - \mathbf{y} + \frac{\varepsilon \mathbf{z}}{2} \right| - \left| \mathbf{z}_r - \mathbf{y} - \frac{\varepsilon \mathbf{z}}{2} \right| = |\mathbf{x}_2 - \mathbf{y}| - |\mathbf{z}_r - \mathbf{y}| + \frac{\varepsilon \mathbf{z}}{2} \cdot \left(\frac{\mathbf{x}_2 - \mathbf{y}}{|\mathbf{x}_2 - \mathbf{y}|} + \frac{\mathbf{z}_r - \mathbf{y}}{|\mathbf{z}_r - \mathbf{y}|} \right) + O(\varepsilon^2).$$

Therefore we have

$$\begin{aligned} \Delta C_I^{(1)}(\tau, \mathbf{x}_1, \mathbf{x}_2) &= \frac{\sigma_r l_r^3 \varepsilon}{2^7 \pi^4 c_0^2} \iiint d\mathbf{y} d\mathbf{z} d\omega \frac{\omega^2 \hat{F}(\omega) K(\mathbf{y}) H(\mathbf{z})}{|\mathbf{x}_1 - \mathbf{z}_r| |\mathbf{z}_r - \mathbf{y}| |\mathbf{x}_2 - \mathbf{y}|} e^{i \frac{\Phi_I(\omega, \mathbf{y})}{\varepsilon}} e^{i \omega \mathbf{z} \cdot \boldsymbol{\kappa}(\mathbf{y})} \\ &= \frac{\sigma_r l_r^3 \varepsilon}{2^7 \pi^4 c_0^2} \iint d\mathbf{y} d\omega \frac{\omega^2 \hat{F}(\omega) K(\mathbf{y}) \hat{H}(\omega \boldsymbol{\kappa}(\mathbf{y}))}{|\mathbf{x}_1 - \mathbf{z}_r| |\mathbf{z}_r - \mathbf{y}| |\mathbf{x}_2 - \mathbf{y}|} e^{i \frac{\Phi_I(\omega, \mathbf{y})}{\varepsilon}}, \end{aligned}$$

where the rapid phase is

$$\Phi_I(\omega, \mathbf{y}) = \omega [\mathcal{T}(\mathbf{x}_2, \mathbf{y}) - \mathcal{T}(\mathbf{x}_1, \mathbf{z}_r) - \mathcal{T}(\mathbf{z}_r, \mathbf{y}) - \tau],$$

and

$$\boldsymbol{\kappa}(\mathbf{y}) = \frac{1}{2c_0} \left(\frac{\mathbf{x}_2 - \mathbf{y}}{|\mathbf{x}_2 - \mathbf{y}|} + \frac{\mathbf{z}_r - \mathbf{y}}{|\mathbf{z}_r - \mathbf{y}|} \right), \quad \kappa(\mathbf{y})^2 = \frac{1}{2c_0^2} \left(1 + \frac{\mathbf{x}_2 - \mathbf{y}}{|\mathbf{x}_2 - \mathbf{y}|} \cdot \frac{\mathbf{z}_r - \mathbf{y}}{|\mathbf{z}_r - \mathbf{y}|} \right).$$

In order to identify the dominant contributions of the first term with the rapid phase Φ_I we apply the stationary phase method. The stationary points satisfy the two conditions

$$\partial_\omega(\Phi_I(\omega, \mathbf{y})) = 0, \quad \nabla_{\mathbf{y}}(\Phi_I(\omega, \mathbf{y})) = \mathbf{0},$$

which means

$$\mathcal{T}(\mathbf{x}_2, \mathbf{y}) - \mathcal{T}(\mathbf{x}_1, \mathbf{z}_r) - \mathcal{T}(\mathbf{z}_r, \mathbf{y}) = \tau, \quad \nabla_{\mathbf{y}} \mathcal{T}(\mathbf{y}, \mathbf{x}_2) = \nabla_{\mathbf{y}} \mathcal{T}(\mathbf{y}, \mathbf{z}_r).$$

The second condition means that \mathbf{x}_2 and \mathbf{z}_r should be on the same ray issued from the source point \mathbf{y} . If $\mathbf{y} \rightarrow \mathbf{x}_2 \rightarrow \mathbf{z}_r$, then the first condition reads $-\mathcal{T}(\mathbf{x}_2, \mathbf{z}_r) - \mathcal{T}(\mathbf{x}_1, \mathbf{z}_r) = \tau$, which is the daylight configuration. If $\mathbf{y} \rightarrow \mathbf{z}_r \rightarrow \mathbf{x}_2$, then the first condition reads $\mathcal{T}(\mathbf{x}_2, \mathbf{z}_r) - \mathcal{T}(\mathbf{x}_1, \mathbf{z}_r) = \tau$, which is the backlight configuration. We focus our attention to the backlight illumination configuration.

We introduce the unit vector

$$\hat{\mathbf{g}}_3 = \frac{\mathbf{z}_r - \mathbf{x}_2}{|\mathbf{z}_r - \mathbf{x}_2|}$$

and complete it with two other unit vectors $(\hat{\mathbf{g}}_1, \hat{\mathbf{g}}_2)$ so that $(\hat{\mathbf{g}}_1, \hat{\mathbf{g}}_2, \hat{\mathbf{g}}_3)$ is an orthonormal basis. We make the change of variables $\mathbf{y} \mapsto (s_1, s_2, s_3)$ with

$$\mathbf{y} = \mathbf{z}_r + |\mathbf{z}_r - \mathbf{x}_2|[s_3\hat{\mathbf{g}}_3 + \varepsilon^{1/2}s_1\hat{\mathbf{g}}_1 + \varepsilon^{1/2}s_2\hat{\mathbf{g}}_2].$$

Its Jacobian is $\varepsilon|\mathbf{z}_r - \mathbf{x}_2|^3$. This gives a parameterization of the variable \mathbf{y} along the ray joining \mathbf{x}_2 and \mathbf{z}_r . Only the terms with $s_3 > 0$ are important in the backlight illumination configuration. We also parameterize the time lag τ around the difference of travel times:

$$\tau = \mathcal{T}(\mathbf{x}_2, \mathbf{z}_r) - \mathcal{T}(\mathbf{x}_1, \mathbf{z}_r) + \varepsilon\tau_0.$$

A Taylor expansion shows that we have

$$\begin{aligned} \Phi_{\text{I}}(\omega, \mathbf{y}) &= -\varepsilon\omega\tau_0 - \varepsilon\omega\frac{s_1^2 + s_2^2}{2c_0s_3(1+s_3)}|\mathbf{x}_2 - \mathbf{z}_r| + O(\varepsilon^2), \\ |\mathbf{x}_1 - \mathbf{z}_r||\mathbf{z}_r - \mathbf{y}||\mathbf{x}_2 - \mathbf{y}| &= |\mathbf{x}_1 - \mathbf{z}_r||\mathbf{z}_r - \mathbf{x}_2|^2s_3(1+s_3) + O(\varepsilon), \\ \kappa(\mathbf{y}) &\simeq \frac{1}{c_0}. \end{aligned}$$

In the last relation we have used the approximation that the distance from the sensor array to the reflector is larger than the diameter of the array. This simplifies the expression but this is not so important: If it is not the case, then the factor $1/c_0$ should be replaced by a factor between $1/(2c_0)$ and $1/c_0$. Using these relations we find

$$\begin{aligned} \Delta C_{\text{I}}^{(1)}(\tau, \mathbf{x}_1, \mathbf{x}_2) &= \frac{\sigma_r l_r^3 |\mathbf{x}_2 - \mathbf{z}_r| \varepsilon^2}{2^7 \pi^4 c_0^2 |\mathbf{x}_1 - \mathbf{z}_r|} \iint ds_3 d\omega \omega^2 \hat{F}(\omega) \hat{H}\left(\frac{\omega}{c_0}\right) \frac{K(\mathbf{z}_r + s_3(\mathbf{z}_r - \mathbf{x}_2))}{s_3(1+s_3)} e^{-i\omega\tau_0} \\ &\quad \times \iint ds_1 ds_2 e^{-i\frac{\omega}{2c_0} \frac{s_1^2 + s_2^2}{s_3(1+s_3)} |\mathbf{x}_2 - \mathbf{z}_r|} \\ &= \frac{\sigma_r l_r^3 \varepsilon^2}{64 \pi^3 c_0 |\mathbf{x}_1 - \mathbf{z}_r|} \left[\int ds_3 K(\mathbf{z}_r + s_3(\mathbf{z}_r - \mathbf{x}_2)) \right] \left[\int d\omega (-i\omega) \hat{F}_H(\omega) e^{-i\omega\tau_0} \right]. \end{aligned}$$

Here we have used the identity

$$\int ds e^{-i\frac{s^2}{2}} = \sqrt{2\pi} e^{-i\frac{\pi}{4}}.$$

Computing in the same way the expression of $\Delta C_{\text{II}}^{(1)}(\tau, \mathbf{x}_1, \mathbf{x}_2)$ we obtain the expression (19).

Appendix C. Proof of Propositions 4.1-4.2

The daylight imaging functional (24) is the sum of two contributions $\mathcal{I}_{\text{I}}^{\text{D}}$ and $\mathcal{I}_{\text{II}}^{\text{D}}$ coming from $\Delta C_{\text{I}}^{(1)}(\tau, \mathbf{x}_j, \mathbf{x}_l)$ and $\Delta C_{\text{II}}^{(1)}(\tau, \mathbf{x}_j, \mathbf{x}_l)$. We first consider $\mathcal{I}_{\text{I}}^{\text{D}}$. We have

$$\Delta C_{\text{I}}^{(1)}(\tau, \mathbf{x}_j, \mathbf{x}_l) = \frac{\sigma_r l_r^3 \varepsilon}{2^7 \pi^4 c_0^2} \iint d\mathbf{y} d\omega \frac{\omega^2 \hat{F}_H(\omega) K(\mathbf{y})}{|\mathbf{x}_j - \mathbf{z}_r| |\mathbf{z}_r - \mathbf{y}| |\mathbf{x}_l - \mathbf{y}|} e^{i\frac{\Phi_{\text{I}}(\omega, \mathbf{y})}{\varepsilon}},$$

where the rapid phase is

$$\Phi_{\text{I}}(\omega, \mathbf{y}) = \omega[\mathcal{T}(\mathbf{x}_l, \mathbf{y}) - \mathcal{T}(\mathbf{x}_j, \mathbf{z}_r) - \mathcal{T}(\mathbf{z}_r, \mathbf{y}) - \tau].$$

The first component of the daylight imaging functional is

$$\mathcal{I}_{\text{I}}^{\text{D}}(\mathbf{z}^S) = \sum_{j,l=1}^N \Delta C_{\text{I}}^{(1)}(-\mathcal{T}(\mathbf{x}_j, \mathbf{z}^S) - \mathcal{T}(\mathbf{x}_l, \mathbf{z}^S), \mathbf{x}_j, \mathbf{x}_l),$$

which reads in the case of a dense array:

$$\mathcal{I}_{\text{I}}^{\text{D}}(\mathbf{z}^S) = \frac{\sigma_{\text{r}} l_{\text{r}}^3 \varepsilon}{2^7 \pi^4 c_0^2 |A|^2} \iint_{A^2} d\mathbf{x} d\mathbf{x}' \iint d\mathbf{y} d\omega \frac{\omega^2 \hat{F}_H(\omega) K(\mathbf{y})}{|\mathbf{x} - \mathbf{z}_r| |\mathbf{z}_r - \mathbf{y}| |\mathbf{x}' - \mathbf{y}|} e^{i \frac{\Phi(\omega, \mathbf{y}, \mathbf{x}, \mathbf{x}')}{\varepsilon}},$$

where the rapid phase is

$$\Phi(\omega, \mathbf{y}, \mathbf{x}, \mathbf{x}') = \omega[\mathcal{T}(\mathbf{x}, \mathbf{z}^S) + \mathcal{T}(\mathbf{x}', \mathbf{z}^S) + \mathcal{T}(\mathbf{x}', \mathbf{y}) - \mathcal{T}(\mathbf{x}, \mathbf{z}_r) - \mathcal{T}(\mathbf{z}_r, \mathbf{y})].$$

The diameter of the array is between the typical wavelength (which is of order ε) and the distance from the array to the reflector (which is of order 1), and we assume here that it is of order $\varepsilon^{1/2}$:

$$a = a_0 \varepsilon^{1/2}.$$

We introduce the orthonormal basis $(\hat{\mathbf{f}}_1, \hat{\mathbf{f}}_2, \hat{\mathbf{f}}_3)$ defined by (25). We parameterize the search point as:

$$\mathbf{z}^S = \mathbf{z}_r + \boldsymbol{\xi}^S = \mathbf{z}_r + \varepsilon^{1/2} \xi_1 \hat{\mathbf{f}}_1 + \varepsilon^{1/2} \xi_2 \hat{\mathbf{f}}_2 + \varepsilon \xi_3 \hat{\mathbf{f}}_3. \quad (\text{C.1})$$

As we will see below this is the correct parameterization in order to get the point spread function, or the resolution, of the daylight imaging functional in the case in which the bandwidth is larger than ε . We make the change of variables $\mathbf{y} \mapsto (s_1, s_2, s_3)$ with

$$\mathbf{y} = |\mathbf{z}_r|[-s_3 \hat{\mathbf{f}}_3 + \varepsilon^{1/2} s_1 \hat{\mathbf{f}}_1 + \varepsilon^{1/2} s_2 \hat{\mathbf{f}}_2],$$

and $(\mathbf{x}, \mathbf{x}') \mapsto (\mathbf{z}, \mathbf{z}')$ with $\mathbf{x} = \varepsilon^{1/2} \mathbf{z}$ and $\mathbf{x}' = \varepsilon^{1/2} \mathbf{z}'$. We carry out Taylor expansions

$$\begin{aligned} |\mathbf{x} - \mathbf{z}^S| - |\mathbf{x} - \mathbf{z}_r| &\simeq \varepsilon \xi_3 - \varepsilon \frac{z_2 \xi_2}{|\mathbf{z}_r|} - \varepsilon \frac{z_1 \xi_1}{|\mathbf{z}_r|} \frac{z_r}{|\mathbf{z}_r|} + \varepsilon \frac{\xi_1^2 + \xi_2^2}{2|\mathbf{z}_r|}, \\ |\mathbf{x}' - \mathbf{z}^S| + |\mathbf{x}' - \mathbf{y}| - |\mathbf{z}_r - \mathbf{y}| &\simeq \varepsilon \xi_3 - \varepsilon \frac{z'_2 \xi_2}{|\mathbf{z}_r|} - \varepsilon \frac{z'_1 \xi_1}{|\mathbf{z}_r|} \frac{z_r}{|\mathbf{z}_r|} + \varepsilon \frac{\xi_1^2 + \xi_2^2}{2|\mathbf{z}_r|} \\ &\quad - \varepsilon \frac{z'_2 s_2}{s_3} - \varepsilon \frac{z'_1 s_1}{s_3} \frac{z_r}{|\mathbf{z}_r|} + \varepsilon \frac{(s_1^2 + s_2^2) |\mathbf{z}_r|}{2s_3(s_3 + 1)} + \varepsilon \frac{z'^2_r}{2|\mathbf{z}_r|^3} \left(1 + \frac{1}{s_3}\right) + \varepsilon \frac{z'^2_2}{2|\mathbf{z}_r|} \left(1 + \frac{1}{s_3}\right). \end{aligned}$$

We compute the integrals in s_1 and s_2

$$\iint e^{i \frac{\omega}{\varepsilon c_0} [|\mathbf{x}' - \mathbf{z}^S| + |\mathbf{x}' - \mathbf{y}| - |\mathbf{z}_r - \mathbf{y}|]} ds_1 ds_2 = \frac{2i\pi c_0 s_3 (1 + s_3)}{\omega |\mathbf{z}_r|} e^{i \frac{\omega}{c_0} [\xi_3 + \frac{\xi_1^2 + \xi_2^2}{2|\mathbf{z}_r|} - \frac{z'_1 \xi_1}{|\mathbf{z}_r|} \frac{z_r}{|\mathbf{z}_r|} - \frac{z'_2 \xi_2}{|\mathbf{z}_r|}]},$$

which gives

$$\iint e^{i \frac{\Phi}{\varepsilon}} ds_1 ds_2 = \frac{2i\pi c_0 s_3 (1 + s_3)}{\omega |\mathbf{z}_r|} e^{i \frac{\omega}{c_0} [2\xi_3 + \frac{\xi_1^2 + \xi_2^2}{|\mathbf{z}_r|} - \frac{z_1 \xi_1}{|\mathbf{z}_r|} \frac{z_r}{|\mathbf{z}_r|} - \frac{z_2 \xi_2}{|\mathbf{z}_r|} - \frac{z'_1 \xi_1}{|\mathbf{z}_r|} \frac{z_r}{|\mathbf{z}_r|} - \frac{z'_2 \xi_2}{|\mathbf{z}_r|}]},$$

and we obtain

$$\mathcal{I}_I^D(\mathbf{z}^S) = \frac{\sigma_r l_r^3 \varepsilon^2 N^2 K_{\mathbf{0}, \mathbf{z}_r}}{2^6 \pi^3 c_0 |\mathbf{z}_r|^2} \int d\omega i \omega \hat{F}_H(\omega) e^{i \frac{\omega}{c_0} [2\xi_3 + \frac{\xi_1^2 + \xi_2^2}{|\mathbf{z}_r|}]} \mathcal{J}_{\alpha_r} \left(\frac{\omega a_0}{c_0 |\mathbf{z}_r|} (\xi_1, \xi_2) \right)^2,$$

where

$$\mathcal{J}_{\alpha_r}(\eta_1, \eta_2) = \frac{1}{|A_0|} \int_{A_0} e^{-i(\alpha_r u_1 \eta_1 + u_2 \eta_2)} du_1 du_2 = \mathcal{G}_{\alpha_r}(\eta_1, \eta_2, 0),$$

and the domain A_0 is the rescaled domain $A = aA_0 = \varepsilon^{1/2} a_0 A_0$.

If the function F_H is of the form (29) and the bandwidth B is smaller than the central frequency ω_0 , but larger than ε , then the expression of $\mathcal{I}_I^D(\mathbf{z}^S)$ becomes:

$$\begin{aligned} \mathcal{I}_I^D(\mathbf{z}^S) &= -\frac{\sigma_r l_r^3 \varepsilon^2 N^2 K_{\mathbf{0}, \mathbf{z}_r} \omega_0}{2^5 \pi^2 c_0 |\mathbf{z}_r|^2} \text{Im} \left[F_{H,0} \left(2 \frac{B}{c_0} \xi_3 + \frac{B}{c_0} \frac{\xi_1^2 + \xi_2^2}{|\mathbf{z}_r|} \right) e^{i [2 \frac{\omega_0}{c_0} \xi_3 + \frac{\omega_0}{c_0} \frac{\xi_1^2 + \xi_2^2}{|\mathbf{z}_r|}]} \right. \\ &\quad \left. \times \mathcal{J}_{\alpha_r} \left(\frac{\omega_0 a_0}{c_0 |\mathbf{z}_r|} (\xi_1, \xi_2) \right)^2 \right], \end{aligned}$$

which shows that the slowly varying envelope is

$$\mathcal{I}_I^D(\mathbf{z}^S) = \frac{\sigma_r l_r^3 \varepsilon^2 N^2 K_{\mathbf{0}, \mathbf{z}_r} \omega_0}{2^6 \pi^2 c_0 |\mathbf{z}_r|^2} \left| F_{H,0} \left(2 \frac{B}{c_0} \xi_3 + \frac{B}{c_0} \frac{\xi_1^2 + \xi_2^2}{|\mathbf{z}_r|} \right) \right| \left| \mathcal{J}_{\alpha_r} \left(\frac{\omega_0 a_0}{c_0 |\mathbf{z}_r|} (\xi_1, \xi_2) \right) \right|^2.$$

With a similar computation for \mathcal{I}_{II}^D we obtain the expression (31) of the point spread function given in Proposition 4.2. Note that the assumption that B is larger than ε corresponds to $B \gg B_c$.

In the narrowband case (the ratio of the bandwidth over the central frequency is of order ε or smaller), then the previous calculations show that the point spread function does not depend of ξ_3 in the limit $\varepsilon \rightarrow 0$ with $\boldsymbol{\xi}^S$ parameterized as (C.1). We now parameterize the search point as:

$$\mathbf{z}^S = \mathbf{z}_r + \boldsymbol{\xi}^S = \mathbf{z}_r + \varepsilon^{1/2} \xi_1 \hat{\mathbf{f}}_1 + \varepsilon^{1/2} \xi_2 \hat{\mathbf{f}}_2 + \xi_3 \hat{\mathbf{f}}_3, \quad (\text{C.2})$$

in which the scaling of the longitudinal offset ξ_3 has been changed compared to the previous case. We make the change of variables $\mathbf{y} \rightarrow (s_1, s_2, s_3)$ and $(\mathbf{x}, \mathbf{x}') \rightarrow (\mathbf{z}, \mathbf{z}')$ as above and we carry out Taylor expansions

$$\begin{aligned} |\mathbf{x} - \mathbf{z}^S| - |\mathbf{x} - \mathbf{z}_r| &\simeq \xi_3 - \varepsilon \frac{z_2 \xi_2}{|\mathbf{z}_r| + \xi_3} - \varepsilon \frac{z_1 \xi_1}{|\mathbf{z}_r| + \xi_3} \frac{z_r}{|\mathbf{z}_r|} + \varepsilon \frac{\xi_1^2 + \xi_2^2}{2(|\mathbf{z}_r| + \xi_3)} \\ &\quad - \varepsilon \frac{z_2^2 \xi_3}{2|\mathbf{z}_r|(|\mathbf{z}_r| + \xi_3)} - \varepsilon \frac{z_1^2 \xi_3}{2|\mathbf{z}_r|(|\mathbf{z}_r| + \xi_3)} \frac{z_r^2}{|\mathbf{z}_r|^2}, \\ |\mathbf{x}' - \mathbf{z}^S| + |\mathbf{x}' - \mathbf{y}| - |\mathbf{z}_r - \mathbf{y}| &\simeq \xi_3 - \varepsilon \frac{z'_2 \xi_2}{|\mathbf{z}_r| + \xi_3} - \varepsilon \frac{z'_1 \xi_1}{|\mathbf{z}_r| + \xi_3} \frac{z_r}{|\mathbf{z}_r|} + \varepsilon \frac{\xi_1^2 + \xi_2^2}{2|\mathbf{z}_r|} \\ &\quad - \varepsilon \frac{z'_2 s_2}{s_3} - \varepsilon \frac{z'_1 s_1}{s_3} \frac{z_r}{|\mathbf{z}_r|} + \varepsilon \frac{(s_1^2 + s_2^2) |\mathbf{z}_r|}{2s_3(s_3 + 1)} + \varepsilon \left(\frac{z_1'^2}{2} \frac{z_r^2}{|\mathbf{z}_r|^2} + \frac{z_2'^2}{2} \right) \left(\frac{1}{s_3 |\mathbf{z}_r|} + \frac{1}{|\mathbf{z}_r| + \xi_3} \right). \end{aligned}$$

We compute the integrals in s_1 and s_2 :

$$\begin{aligned} \iint e^{i \frac{\Phi}{\varepsilon}} ds_1 ds_2 &= \frac{2i\pi c_0 s_3 (1 + s_3)}{\omega |\mathbf{z}_r|} e^{i \frac{\omega}{c_0} [2 \frac{\xi_3}{\varepsilon} + \frac{\xi_1^2 + \xi_2^2}{2} (\frac{1}{|\mathbf{z}_r|} + \frac{1}{|\mathbf{z}_r| + \xi_3}) + \lambda(z_1, z_2) + \lambda(z'_1, z'_2)]}, \\ \lambda(z_1, z_2) &= -\frac{z_1 \xi_1}{|\mathbf{z}_r| + \xi_3} \frac{z_r}{|\mathbf{z}_r|} - \frac{z_2 \xi_2}{|\mathbf{z}_r| + \xi_3} - \left(\frac{z_1^2}{2} \frac{z_r^2}{|\mathbf{z}_r|^2} + \frac{z_2^2}{2} \right) \frac{\xi_3}{|\mathbf{z}_r|(|\mathbf{z}_r| + \xi_3)}, \end{aligned} \quad (\text{C.3})$$

and we obtain

$$\begin{aligned} \mathcal{I}_I^D(\mathbf{z}^S) &= \frac{\sigma_r l_r^3 \varepsilon^2 N^2 K_{\mathbf{0}, \mathbf{z}_r}}{2^6 \pi^3 c_0 |\mathbf{z}_r|^2} \int d\omega i\omega \hat{F}_H(\omega) e^{i\frac{\omega}{\varepsilon c_0} [2\xi_3]} e^{i\frac{\omega}{c_0} \frac{\xi_1^2 + \xi_2^2}{2} [\frac{1}{|\mathbf{z}_r|} + \frac{1}{|\mathbf{z}_r| + \xi_3}]} \\ &\quad \times \mathcal{G}_{\alpha_r} \left(\frac{\omega a_0}{c_0 (|\mathbf{z}_r| + \xi_3)} \xi_1, \frac{\omega a_0}{c_0 (|\mathbf{z}_r| + \xi_3)} \xi_2, \frac{\omega a_0^2}{c_0 |\mathbf{z}_r| (|\mathbf{z}_r| + \xi_3)} \xi_3 \right)^2, \end{aligned}$$

where \mathcal{G}_{α_r} is the normalized profile defined by (27). When $|\xi_3| \ll |\mathbf{z}_r|$ this gives (with a similar computation for \mathcal{I}_{II}^D) the expression (28) of the point spread function as stated in Proposition 4.1. If we assume that the bandwidth is of the order of ε :

$$\hat{F}_H(\omega) = \frac{1}{2\varepsilon B_0} \left[\hat{F}_{H,0} \left(\frac{\omega_0 - \omega}{\varepsilon B_0} \right) + \hat{F}_{H,0} \left(\frac{\omega_0 + \omega}{\varepsilon B_0} \right) \right],$$

then the expression of $\mathcal{I}_I^D(\mathbf{z}^S)$ becomes

$$\begin{aligned} \mathcal{I}_I^D(\mathbf{z}^S) &= -\frac{\sigma_r l_r^3 \varepsilon^2 N^2 K_{\mathbf{0}, \mathbf{z}_r} \omega_0}{2^5 \pi^2 c_0 |\mathbf{z}_r|^2} \text{Im} \left[F_{H,0} \left(\frac{2B_0 \xi_3}{c_0} \right) e^{i2\frac{\omega_0}{c_0 \varepsilon} \xi_3 + i\frac{\omega_0}{c_0} \frac{\xi_1^2 + \xi_2^2}{2} [\frac{1}{|\mathbf{z}_r|} + \frac{1}{|\mathbf{z}_r| + \xi_3}]} \right. \\ &\quad \left. \times \mathcal{G}_{\alpha_r} \left(\frac{\omega_0 a_0}{c_0 (|\mathbf{z}_r| + \xi_3)} \xi_1, \frac{\omega_0 a_0}{c_0 (|\mathbf{z}_r| + \xi_3)} \xi_2, \frac{\omega_0 a_0^2}{c_0 |\mathbf{z}_r| (|\mathbf{z}_r| + \xi_3)} \xi_3 \right)^2 \right], \end{aligned}$$

whose slowly varying envelope is

$$\begin{aligned} \mathcal{I}_I^D(\mathbf{z}^S) &= \frac{\sigma_r l_r^3 \varepsilon^2 N^2 K_{\mathbf{0}, \mathbf{z}_r} \omega_0}{2^6 \pi^2 c_0 |\mathbf{z}_r|^2} \left| F_{H,0} \left(\frac{2B_0 \xi_3}{c_0} \right) \right| \\ &\quad \times \left| \mathcal{G}_{\alpha_r} \left(\frac{\omega_0 a_0}{c_0 (|\mathbf{z}_r| + \xi_3)} \xi_1, \frac{\omega_0 a_0}{c_0 (|\mathbf{z}_r| + \xi_3)} \xi_2, \frac{\omega_0 a_0^2}{c_0 |\mathbf{z}_r| (|\mathbf{z}_r| + \xi_3)} \xi_3 \right) \right|^2. \end{aligned}$$

When $B_0 \ll 1$ (which means $B \ll B_c$) and $|\xi_3| \ll |\mathbf{z}_r|$ we obtain the expression (32) given in Proposition 4.2.

Appendix D. Proof of Proposition 4.3

Let us consider the backlight imaging functional and proceed as in the previous appendix for the proof of Proposition 4.1. The backlight imaging functional is the sum of the contributions \mathcal{I}_I^B and \mathcal{I}_{II}^B from ΔC_I and ΔC_{II} . We first remark that the contribution $\mathcal{I}_{II}^B(\mathbf{z}^S) = \overline{\mathcal{I}_I^B(\mathbf{z}^S)}$ and we concentrate our attention to $\mathcal{I}_I^B(\mathbf{z}^S)$. We parameterize the search point as follows:

$$\mathbf{z}^S = \mathbf{z}_r + \varepsilon^{1/2} \xi_1 \hat{\mathbf{f}}_1 + \varepsilon^{1/2} \xi_2 \hat{\mathbf{f}}_2 + \xi_3 \hat{\mathbf{f}}_3.$$

In the integral representation of \mathcal{I}_I^D we make the change of variables $\mathbf{y} \mapsto (s_1, s_2, s_3)$ with

$$\mathbf{y} = |\mathbf{z}_r| [s_3 \hat{\mathbf{f}}_3 + \varepsilon^{1/2} s_1 \hat{\mathbf{f}}_1 + \varepsilon^{1/2} s_2 \hat{\mathbf{f}}_2],$$

and $(\mathbf{x}, \mathbf{x}') \mapsto (\mathbf{z}, \mathbf{z}')$ with $\mathbf{x} = \varepsilon^{1/2} \mathbf{z}$ and $\mathbf{x}' = \varepsilon^{1/2} \mathbf{z}'$. We carry out Taylor expansions

$$\begin{aligned} |\mathbf{x} - \mathbf{z}^S| - |\mathbf{x} - \mathbf{z}_r| &\simeq \xi_3 - \varepsilon \frac{z_2 \xi_2}{|\mathbf{z}_r| + \xi_3} - \varepsilon \frac{z_1 \xi_1}{|\mathbf{z}_r| + \xi_3} \frac{z_r}{|\mathbf{z}_r|} + \varepsilon \frac{\xi_1^2 + \xi_2^2}{2(|\mathbf{z}_r| + \xi_3)} \\ &\quad - \varepsilon \frac{z_2^2 \xi_3}{2|\mathbf{z}_r| (|\mathbf{z}_r| + \xi_3)} - \varepsilon \frac{z_1^2 \xi_3}{2|\mathbf{z}_r| (|\mathbf{z}_r| + \xi_3)} \frac{z_r^2}{|\mathbf{z}_r|^2}, \end{aligned}$$

$$\begin{aligned}
-|\mathbf{x}' - \mathbf{z}^S| + |\mathbf{x}' - \mathbf{y}| - |\mathbf{z}_r - \mathbf{y}| &\simeq -\xi_3 + \varepsilon \frac{z'_2 \xi_2}{|\mathbf{z}_r| + \xi_3} + \varepsilon \frac{z'_1 \xi_1}{|\mathbf{z}_r| + \xi_3} \frac{z_r}{|\mathbf{z}_r|} - \varepsilon \frac{\xi_1^2 + \xi_2^2}{2(|\mathbf{z}_r| + \xi_3)} \\
&- \varepsilon \frac{z'_2 s_2}{s_3} - \varepsilon \frac{z'_1 s_1}{s_3} \frac{z_r}{|\mathbf{z}_r|} - \varepsilon \frac{(s_1^2 + s_2^2) |\mathbf{z}_r|}{2s_3(s_3 - 1)} + \varepsilon \left(\frac{z_1'^2}{2} \frac{z_r^2}{|\mathbf{z}_r|^2} + \frac{z_2'^2}{2} \right) \left(\frac{1}{s_3 |\mathbf{z}_r|} - \frac{1}{|\mathbf{z}_r| + \xi_3} \right).
\end{aligned}$$

We compute the integrals in s_1 and s_2 :

$$\iint e^{i\frac{\Phi}{\varepsilon}} ds_1 ds_2 = -\frac{2i\pi c_0 s_3 (s_3 - 1)}{\omega |\mathbf{z}_r|} e^{i\frac{\omega}{c_0} [\lambda(z_1, z_2) - \lambda(z'_1, z'_2)]},$$

where λ is defined by (C.3), and we obtain

$$\begin{aligned}
\mathcal{I}_1^B(\mathbf{z}^S) &= -\frac{\sigma_r l_r^3 \varepsilon^2 N^2 K_{\mathbf{z}_r, \mathbf{0}}}{2^6 \pi^3 c_0 |\mathbf{z}_r|^2} \int d\omega i\omega \hat{F}_H(\omega) \\
&\times \left| \mathcal{G}_{\alpha_r} \left(\frac{\omega a_0}{c_0 (|\mathbf{z}_r| + \xi_3)} \xi_1, \frac{\omega a_0}{c_0 (|\mathbf{z}_r| + \xi_3)} \xi_2, \frac{\omega a_0^2}{c_0 |\mathbf{z}_r| (|\mathbf{z}_r| + \xi_3)} \xi_3 \right) \right|^2.
\end{aligned}$$

However the function \hat{F}_H and the term in the second line are even functions in ω so that this contribution is in fact 0. It is necessary to perform a higher-order expansion in ε to get the leading-order term. By doing this we obtain

$$\begin{aligned}
\mathcal{I}_1^B(\mathbf{z}^S) &= -\frac{\sigma_r l_r^3 \varepsilon^{5/2} N^2 (|\mathbf{z}_r| + \xi_3)}{2^4 \pi^3 |\mathbf{z}_r|^2} \int d\omega \hat{F}_H(\omega) \\
&\times \left[\frac{|\mathbf{z}_r|}{z_r} \partial_{x_1} K_{\mathbf{z}_r, \mathbf{0}} \partial_{\xi_1} + \partial_{x_2} K_{\mathbf{z}_r, \mathbf{0}} \partial_{\xi_2} \right] \left| \mathcal{G}_{\alpha_r} \left(\frac{\omega a_0}{c_0 (|\mathbf{z}_r| + \xi_3)} \xi_1, \frac{\omega a_0}{c_0 (|\mathbf{z}_r| + \xi_3)} \xi_2, \frac{\omega a_0^2}{c_0 |\mathbf{z}_r| (|\mathbf{z}_r| + \xi_3)} \xi_3 \right) \right|^2.
\end{aligned}$$

The end of the proof is then similar to the one of Proposition 4.1 for the daylight imaging functional.

- [1] C. BARDOS, J. GARNIER, AND G. PAPANICOLAOU, *Identification of Green's functions singularities by cross correlation of noisy signals*, Inverse Problems, 24 (2008), 015011.
- [2] B. L. BIONDI, *3D Seismic Imaging*, no. 14 in Investigations in Geophysics, Society of Exploration Geophysics, Tulsa, 2006.
- [3] N. BLEISTEIN, J. K. COHEN, AND J. W. STOCKWELL JR, *Mathematics of multidimensional seismic imaging, migration, and inversion*, Springer Verlag, New York, 2001.
- [4] L. BORCEA, G. PAPANICOLAOU, AND C. TSOGKA, *Theory and applications of time reversal and interferometric imaging*, Inverse Problems, 19 (2003), pp. S134-S164.
- [5] M. BORN AND E. WOLF, *Principles of optics*, Cambridge University Press, Cambridge, 1999.
- [6] F. BRENGUIER, N. M. SHAPIRO, M. CAMPILLO, V. FERRAZZINI, Z. DUPUTEL, O. COUTANT, AND A. NERCESSIAN, *Towards forecasting volcanic eruptions using seismic noise*, Nature Geoscience, 1 (2008), pp. 126-130.
- [7] Y. COLIN DE VERDIÈRE, *Semiclassical analysis and passive imaging*, Nonlinearity, 22 (2009), pp. R45-R75.
- [8] A. CURTIS, P. GERSTOFT, H. SATO, R. SNIEDER, AND K. WAPENAAR, *Seismic interferometry - turning noise into signal*, The Leading Edge, 25 (2006), pp. 1082-1092.
- [9] M. DE HOOP AND K. SØLNA, *Estimating a Green's function from field-field correlations in a random medium*, SIAM J. Appl. Math., 69 (2009), pp. 909-932.
- [10] T. L. DUVAL JR, S. M. JEFFERIES, J. W. HARVEY, AND M. A. POMERANTZ, *Time-distance helioseismology*, Nature, 362 (1993), pp. 430-432.
- [11] J.-P. FOUQUE, J. GARNIER, G. PAPANICOLAOU, AND K. SØLNA, *Wave propagation and time reversal in randomly layered media*, Springer, New York, 2007.
- [12] J. GARNIER AND G. PAPANICOLAOU, *Passive sensor imaging using cross correlations of noisy signals in a scattering medium*, SIAM J. Imaging Sciences, 2 (2009), pp. 396-437.

- [13] J. GARNIER AND K. SØLNA, *Cross correlation and deconvolution of noise signals in randomly layered media*, to appear in SIAM J. Imaging Sciences.
- [14] P. GOUÉDARD, L. STEHLY, F. BRENGUIER, M. CAMPILLO, Y. COLIN DE VERDIÈRE, E. LAROSE, L. MARGERIN, P. ROUX, F. J. SANCHEZ-SESMA, N. M. SHAPIRO, AND R. L. WEAVER, *Cross-correlation of random fields: mathematical approach and applications*, Geophysical Prospecting, 56 (2008), pp. 375-393.
- [15] E. LAROSE, L. MARGERIN, A. DERODE, B. VAN TIGGELEN, M. CAMPILLO, N. SHAPIRO, A. PAUL, L. STEHLY, AND M. TANTER, *Correlation of random wave fields: an interdisciplinary review*, Geophysics, 71 (2006), pp. SI11-SI21.
- [16] J. RICKETT AND J. CLAERBOUT, *Acoustic daylight imaging via spectral factorization: Helioseismology and reservoir monitoring*, The Leading Edge, 18 (1999), pp. 957-960.
- [17] K. G. SABRA, P. GERSTOFT, P. ROUX, AND W. KUPERMAN *Surface wave tomography from microseisms in Southern California* Geophys. Res. Lett., 32 (2005), L14311.
- [18] K. G. SABRA, P. ROUX, P. GERSTOFT, W. A. KUPERMAN, M. C. FEHLER, *Extracting coherent coda arrivals from cross correlations of long period seismic waves during the Mount St Helens 2004 eruption*, Geophys. Res. Lett., 33 (2006), L06313.
- [19] G. T. SCHUSTER, J. YU, J. SHENG, AND J. RICKETT, *Interferometric daylight seismic imaging*, Geophysical Journal International, 157 (2004), pp. 832-852.
- [20] N. M. SHAPIRO, M. CAMPILLO, L. STEHLY, AND M. H. RITZWOLLER, *High-resolution surface wave tomography from ambient noise*, Science, 307 (2005), pp. 1615-1618.
- [21] L. STEHLY, M. CAMPILLO, AND N. M. SHAPIRO, *A study of the seismic noise from its long-range correlation properties*, Geophys. Res. Lett., 111 (2006), B10306.
- [22] L. STEHLY, M. CAMPILLO, B. FROMENT, AND R. WEAVER, *Reconstructing Greens function by correlation of the coda of the correlation (C3) of ambient seismic noise*, J. Geophys. Res., 113 (2008), B11306.
- [23] H. YAO, R. D. VAN DER HILST, AND M. V. DE HOOP, *Surface-wave array tomography in SE Tibet from ambient seismic noise and two-station analysis I. Phase velocity maps*, Geophysical Journal International, 166 (2006), pp. 732-744.